EXPERIMENTAL AND NUMERICAL INVESTIGATION OF BUCKLING RESTRAINED BRACES

A THESIS SUBMITTED TO
THE GRADUATE SCHOOL OF NATURAL AND APPLIED SCIENCES
OF
MIDDLE EAST TECHNICAL UNIVERSITY

BY

MEHMET EMRAH ERYAŞAR

IN PARTIAL FULFILLMENT OF THE REQUIREMENTS
FOR
THE DEGREE OF MASTER OF SCIENCE
IN
CIVIL ENGINEERING

FEBRUARY 2009

Approval of the thesis:

EXPERIMENTAL AND NUMERICAL STUDY OF BUCKLING RESTRAINED BRACES

submitted by **MEHMET EMRAH ERYAŞAR** in partial fulfillment of the requirements for the degree of **Master of Science in Civil Engineering Department, Middle East Technical University** by,

Prof. Dr. Canan Özgen _____
Dean, Graduate School of **Natural and Applied Sciences**

Prof. Dr. Güney Özcebe _____
Head of Department, **Civil Engineering**

Assoc. Prof. Dr. Cem Topkaya _____
Supervisor, **Civil Engineering Dept., METU**

Examining Committee Members:

Prof. Dr. Polat Gülkan _____
Civil Engineering Dept., METU

Assoc. Prof. Dr. Cem Topkaya _____
Civil Engineering Dept., METU

Prof. Dr. Mehmet Utku _____
Civil Engineering Dept., METU

Prof. Dr. Güney Özcebe _____
Civil Engineering Dept., METU

Assoc. Prof. Dr. Murat Dicleli _____
Engineering Sciences Dept., METU

Date: 11.02.2009

I hereby declare that all information in this document has been obtained and presented in accordance with academic rules and ethical conduct. I also declare that, as required by these rules and conduct, I have fully cited and referenced all material and results that are not original to this work.

Name, Last name : Mehmet Emrah, Eryaşar

Signature :

ABSTRACT

EXPERIMENTAL AND NUMERICAL INVESTIGATION OF BUCKLING RESTRAINED BRACES

Eryaşar, Mehmet Emrah
M.Sc., Department of Civil Engineering
Supervisor : Assoc. Prof. Dr. Cem Topkaya

February 2009, 65 pages

A typical buckling restrained brace (BRB) consists of a core segment and a buckling restraining mechanism. When compared to a conventional brace, BRBs provide nearly equal axial yield force in tension and compression. Buckling restraining mechanism can be grouped into two main categories. Buckling is inhibited either by using a concrete or mortar filled steel tube or by using steel sections only. While a large body of knowledge exists on buckling restrained braces, the behavior of steel encased BRBs has not been studied in detail. Another area that needs further investigation is the detailing of the debonding material. For all types of BRBs, a debonding material or a gap has to be utilized between the core brace and the restraining mechanism. The main function of the debonding material is to eliminate the transfer of shear force between the core brace and the restraining mechanism by preventing or reducing the friction. A two phase research study has been undertaken to address these research needs. In the first phase an experimental study was carried out to investigate the potential of using steel encased BRBs. In the second phase a numerical study was conducted to study the friction problem in BRBs. The experimental study revealed that steel encased braces provide stable hysteretic behavior and can be an alternative to mortar filled steel tubes. Material and geometric properties of the debonding layer for desired axial load behavior were identified and are presented herein.

Keywords: Buckling Restrained Brace, Hysteretic Damper, Friction, Finite Element Method, Debonding

ÖZ

BURKULMASI ÖNLENMİŞ ÇAPRAZLARIN DENEYSEL VE NÜMERİK OLARAK İNCELENMESİ

Eryaşar, Mehmet Emrah
Yüksek Lisans, İnşaat Mühendisliği Bölümü
Tez Yöneticisi : Doç. Dr. Cem Topkaya

Şubat 2009, 65 sayfa

Tipik bir burkulması önlenmiş çapraz çekirdek parçası ve burkulmayı önleyici mekanizmadan oluşmaktadır. Normal çaprazlarla kıyaslandıklarında, burkulması önlenmiş çaprazlar çekme ve basınç altında nerdeyse eşit yüklerde akmaktadırlar. Burkulmayı önleyici mekanizmalar genel olarak iki gruptan oluşmaktadır. Birinci grupta beton veya çimento harcı doldurulmuş kutu profiller kullanılarak, ikinci grupta ise sadece çelik profiller kullanılarak burkulma engellenmektedir. Burkulması önlenmiş çaprazların davranışı hakkında geniş bilgiye sahip olunsada, çelik profiller kullanılan mekanizmalarla ilgili detaylı çalışma bulunmamaktadır. Araştırılması gereken diğer bir konu ise çekirdek parça ile burkulmayı önleyen mekanizmanın arasında oluşan sürtünmeyi engelleyerek ya da azaltarak kesme kuvveti aktarılmamasını sağlayan bir ayırıcı malzemenin detaylandırılmasıdır. Bahsedilen konuları kapsayan iki aşamalı bir çalışma yapılmıştır. Birinci aşama çelik profiller kullanılarak oluşturulan burkulmayı önleyici mekanizmaların deneysel olarak incelenmesidir. İkinci aşamada ise numerik bir çalışma yürütülmüş olup burkulması önlenmiş çaprazlarda gözlenen sürtünme problemi çalışılmıştır. Deneysel çalışmalar çelik profiller ile oluşturulan mekanizmaların düzgün histeretik davranış sağladığını ve çimento harcı doldurulmuş kutu profillere alternatif olabileceğini göstermiştir. İstenilen eksenel yük davranışı için ayırıcı tabakanın malzeme ve geometrik özellikleri belirlenmiş ve sunulmuştur.

Anahtar Kelimeler: Burkulması Önlenmiş Çapraz, Histeretik Sönümleyici, Sürtünme, Sonlu Elemanlar Metodu, Ayırıcı

ACKNOWLEDGMENTS

The author wishes to express his deepest gratitude to his supervisor Assoc. Prof. Dr. Cem Topkaya for his invaluable assistance, guidance and insight throughout the research.

Many thanks also go to all his graduate friends, especially colleagues; Can Karageyik, Efe Gökçe Kurt and Mustafa Emre Özkök for their support. Not forgetting to his bestfriends who always been there.

The technical assistance of Mr. Osman Keskin is gratefully acknowledged.

The author wishes to express his gratitude to his family; his father, Elvan Eryaşar, his mother Mine Eryaşar, and his brother Emre Eryaşar for their understanding and invaluable support throughout his studies.

Lastly, but not leastly, the author would like to give his special thanks to his love Pelin for the moral support she provided throughout his research. Without her loving support and understanding it would have been almost impossible to complete this study.

This study was supported by contracts from the College of Engineering, Middle East Technical University (BAP 2008-03-03-03) and the Scientific & Technological Research Council of Turkey (TÜBİTAK – 105M242). Opinions expressed in this thesis are those of the author and do not reflect the views of the sponsors.

TABLE OF CONTENTS

CHAPTER 1

INTRODUCTION

1.1 Background

Frames with buckling restrained braces (BRBs) can be used as a seismic load resistance system. A typical BRB consists of a core segment and a buckling restraining mechanism. When compared to a conventional brace, BRBs provide nearly equal axial yield force in tension and compression. In addition, BRBs exhibit stable and predictable hysteretic behavior, provide significant energy dissipation capacity and ductility (Fig. 1.1). These braces plasticize during a moderate to severe earthquakes and can be considered as hysteretic dampers.

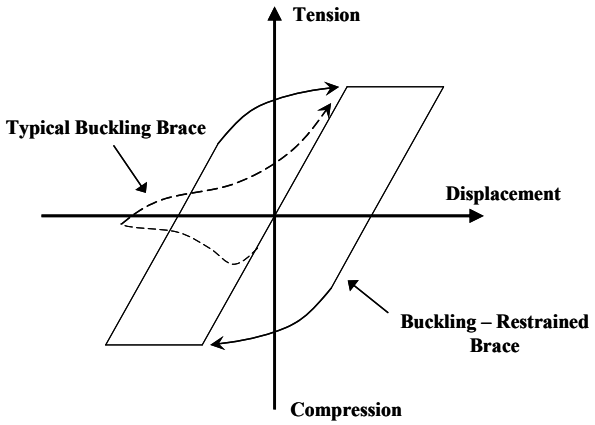

Figure 1.1 – Comparison of Behavior between a Typical Buckling Brace and a BRB

A significant amount of research work has been performed in Japan and elsewhere in Asia over the last few decades for the development of BRBs (Xie, 2005). A detailed summary of findings are summarized in an excellent report by Uang and Nakashima (2004). A number of different restraining mechanisms have been developed that can be grouped into two main categories. In the majority of the braces produced, buckling is inhibited by a concrete or mortar filled steel encasing member which is

usually a hollow structural section (HSS). The other alternative is to restrain the core brace utilizing steel sections. Each type has certain advantages and disadvantages. Mortar filled tubes were found to have problems concerning the quality control in manufacturing process and flexibility in the design details at both ends of the core plate (Iwata et al., 2006). On the other hand, steel encasing alone were found to provide inadequate hysteresis under high strains (Iwata et al., 2000). Most of the BRBs developed to date are proprietary. A survey of existing buildings (Black et al., 2002) revealed that most of the BRBs used so far utilize mortar filled tubes as encasing members.

Proprietary BRBs that have been developed in Japan are treated as hysteretic dampers in design, and no design provisions are available (Uang and Nakashima, 2004). In the United States, however, design recommendations have recently been incorporated into AISC 341-05 Seismic Provisions for Structural Steel Buildings (2005). This provision requires qualifying cyclic tests to be performed on a subassemblage and a uniaxial test specimen. For the design of bracing connections and adjoining members, AISC 341-05 specification requires the use of adjusted brace strength (P_{abs}) which is defined as follows:

$$\begin{aligned} P_{abs} &= \beta\omega P_{ysc} \quad \text{in compression} \\ P_{abs} &= \omega P_{ysc} \quad \text{in tension} \\ P_{ysc} &= F_{ysc} A_{sc} \end{aligned} \tag{1.1}$$

where, F_{ysc}: actual yield stress of the steel core as determined from a coupon test; A_{sc}: net area of steel core; β: compression strength adjustment factor; ω: strain hardening adjustment factor.

The adjustment factors β and ω which are solely dependent on BRB details are determined by testing. When subjected to strong ground shaking, BRB members can experience axial strains that are 10 to 20 times their yield strain. During any inelastic excursion cyclic hardening of the core material takes place which in turn increases the brace force beyond the yield force, P_{ysc}. Furthermore, due to manufacturing details, certain amount of friction that develops between the core segment and the buckling-restraining mechanism is inevitable. Transfer of frictional forces also results in an increase in the brace force. The strain hardening adjustment factor, ω, is calculated as the ratio of the maximum tension force measured from the qualification tests to the yield force, P_{ysc}, of the test specimen. When a BRB is subjected to compression, lateral expansion of the steel core takes place due to Poisson's effect. The area of the steel core

and the frictional resistance due to contact increase as a result of lateral expansion. Because of this Poisson's effect compressive force level attained is higher than the tensile load level for the same amount of axial displacement. The compression strength adjustment factor, β, is calculated as the ratio of the maximum compression force to the maximum tension force of the test specimen. AISC Seismic Provisions mandate that the compression strength adjustment factor, β, be less than 1.3 for each displacement excursion greater than the yield displacement.

1.2 Problem Statement

While a large body of knowledge exists on buckling restrained braces the behavior of steel encased BRBs has not been studied in detail. In a recent study by Tremblay et al. (2006) the authors concluded that steel encased BRBs have a potential for adequate ductile seismic response. However, their test results indicated the necessity to control local core buckling response to minimize frictional response between the core and the buckling-restraining mechanism and develop uniform strain demand in the core segment. Moreover, author concluded that further research is needed to study the effects of unbonding material on the global response. Based on this discussion it is apparent that a detailed investigation on the steel encased BRBs is needed.

Another area that needs further investigation is the detailing of the debonding material. For all types of BRBs a debonding material or a gap must be utilized between the core brace and the restraining mechanism. The main function of the debonding material is to eliminate the transfer of shear force between the core brace and the restraining mechanism. Materials like rubber (Murakami et al., 1999, Iwata et al., 2000, Staker and Reaveley, 2002), polyethylene (Tada et al., 1993 and Manabe et al., 1996, Tremblay et al. 1999), silicon grease (Inoue et al., 1992 and Suzuki et al., 1994, Chen et al. 2001a), or mastic tape (Fujimoto et al., 1988, Watanabe et al., 1988 and Saeki et al., 1995) have been reported in the past. A debonding material or a gap is also needed to accommodate the expansion of the steel core segment. Under compressive forces, the steel core expands in both transverse directions due to Poisson's effect. The thickness of the debonding material or the amount of gap should be large enough to allow for this expansion. Otherwise the friction that is created by the bearing action between the core brace and the restraining mechanism would force the latter to carry some axial load. On the other hand, if the thickness of the debonding material or the amount of gap is too large, the core segment can locally buckle resulting in a reduced low-cycle fatigue life.

A two phase research study has been undertaken to address these research needs. In the first phase an experimental study was carried out to investigate the potential of using steel encased BRBs. In the second phase a numerical study was conducted to study the friction problem in BRBs.

The experimental part of the research program is given in Chapter 2. Following this chapter the details of the numerical study are presented in Chapter 3. Finally, conclusions are given in Chapter 4.

CHAPTER 2

EXPERIMENTAL STUDY ON STEEL ENCASED BUCKLING RESTRAINED BRACES

2.1 Objectives

An experimental study was carried out with the following objectives: (i) investigate the potential use of steel encasing in BRBs; (ii) evaluate the use of welded or bolted attachments for buckling-restraining mechanisms; (iii) examine the effects of attachment details in particular the level of bolt pretension on the compressive strength adjustment and strain hardening adjustment factors; (iv) assess the use of rolled or built-up shapes as steel encasing; (v) evaluate the consequences of imperfections due to manufacturing; (vi) investigate the performance of core segments with different aspect ratios. A total of twelve tests were performed on small scale BRB specimens. The details of the experimental program and the results are presented herein.

2.2 Test Setup and Loading Protocol

A self contained test setup shown in Figs 2.1 and 2.2 were used in the experimental program. The test setup consists of a frame which is specifically built for this project. Tensile and compressive loads are applied to the specimen by making use of a 250 kN screw jack. The screw jack is driven by a motor which is controlled through a frequency inverter. A 200 kN capacity load cell is mounted on the screw jack to measure the level of axial loads.

Core segment to buckling-restraining mechanism attachment detail was investigated as a part of this study. Therefore, BRB specimens were tested vertically to observe slipping of the encasing segment. The total length of BRB specimens was 1140 mm. All BRB specimens had cruciform type nonyielding segments at both ends and a 900 mm long restrained yielding segment. During a typical experiment axial displacements of the restrained yielding segment were monitored by making use of two 50 mm stroke string potentiometers with 0.01 mm accuracy. These potentiometers were placed on both sides of the specimen by welding attachment rods to the nonyielding cruciform segment. Axial load and displacement measurements were collected at every

2 seconds using a digital data acquisition system. The average of the two displacement readings was used to monitor the axial displacement.

All specimens were subjected to a stepwise incremental quasi-static loading protocol. AISC Seismic Provisions (2005) presents a loading protocol to be used in qualifying cyclic BRB tests. The AISC procedure is based on the deformation quantity at first significant yield (Δ_{by}) and the deformation quantity corresponding to design story drift (Δ_{bm}). According to the AISC procedure specimens are cycled at increasing axial displacements up to two times the deformation corresponding to the design story drift (Δ_{bm}). In the present study a similar yet slightly different loading protocol was adopted for the brace experiments. A displacement value at design level needs to be assumed to construct a loading protocol. In an excellent paper by Tremblay et al. (2006), researchers studied the anticipated strain demand on the brace core. These researchers demonstrated that the strain demand is influenced by several geometric, material factors and seismic design characteristics of the structure. Nonetheless, Tremblay et al. (2006) have shown that the strain demand generally remains within the range of 1 to 2 percent unless the brace core is made significantly shorter, in which core strain values up to 3 to 5 percent can be expected.

In the present study, the strain demand at the design level was taken as 1 percent. A loading protocol shown in Fig. 2.3 was adopted. In this loading protocol specimens were cycled at 8 different axial displacement levels which are 1/3 of the yield displacement, 2/3 of the yield displacement, the yield displacement, and displacements corresponding to 0.33 Δ_{bm} (0.33%), 0.5 Δ_{bm} (0.5%), 1.0 Δ_{bm} (1%), 1.5 Δ_{bm} (1.5%), and 2 Δ_{bm} (2%). Two cycles of loading were applied at each displacement level. For the yield strength values used in the present study this loading protocol produces cumulative axial deformation levels in excess of 200 times the yield displacement as required by the AISC Seismic Provisions (2005). The difference between the adopted loading protocol and the one recommended by AISC stems from the presence of early cycles (before yield) and the cycle at twice the yield displacement.

Loading was applied slowly due to the limited motor speed and the need to closely monitor the behavior of specimens. The total time to complete one test ranged between 3 to 4 hours. The strain rate in the core segment of the brace was 55 με/sec.

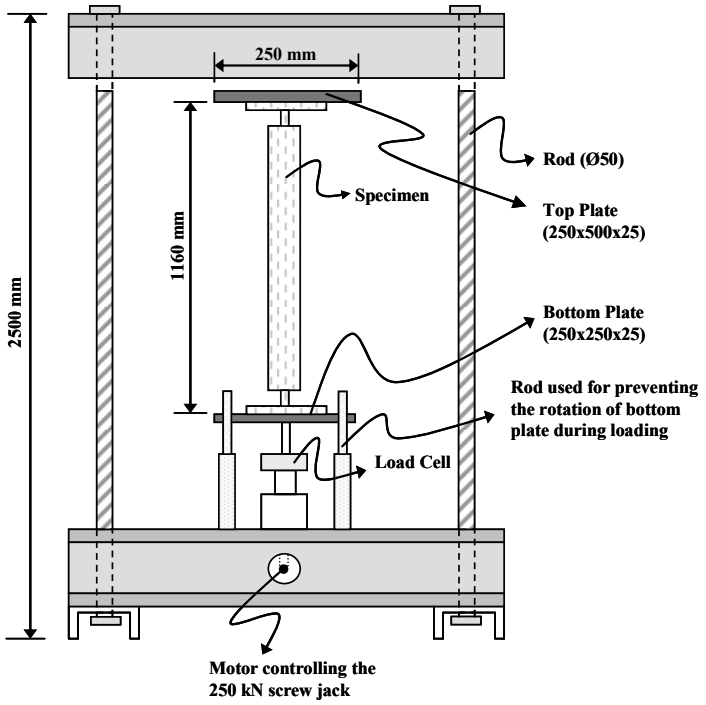

Front View

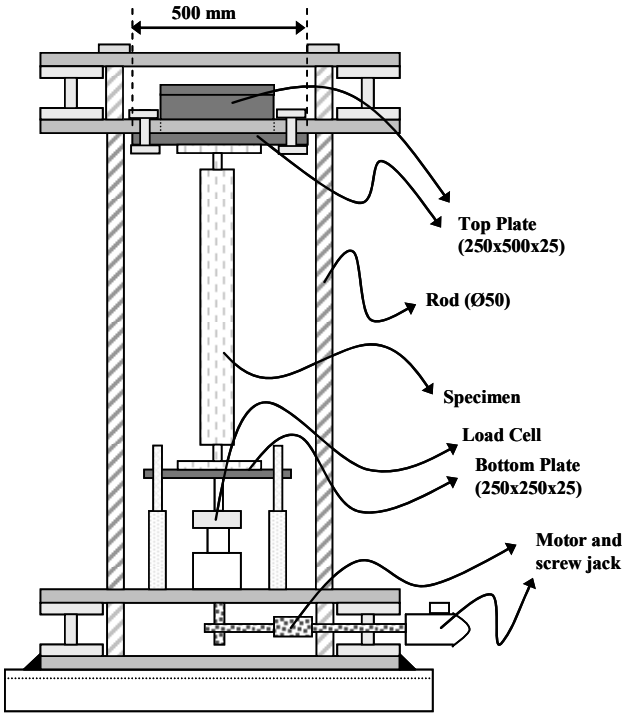

Side View

Figure 2.1 - Representative Drawing of the Test Setup (Not to Scale)

Figure 2.2 – Photo of the Test Setup

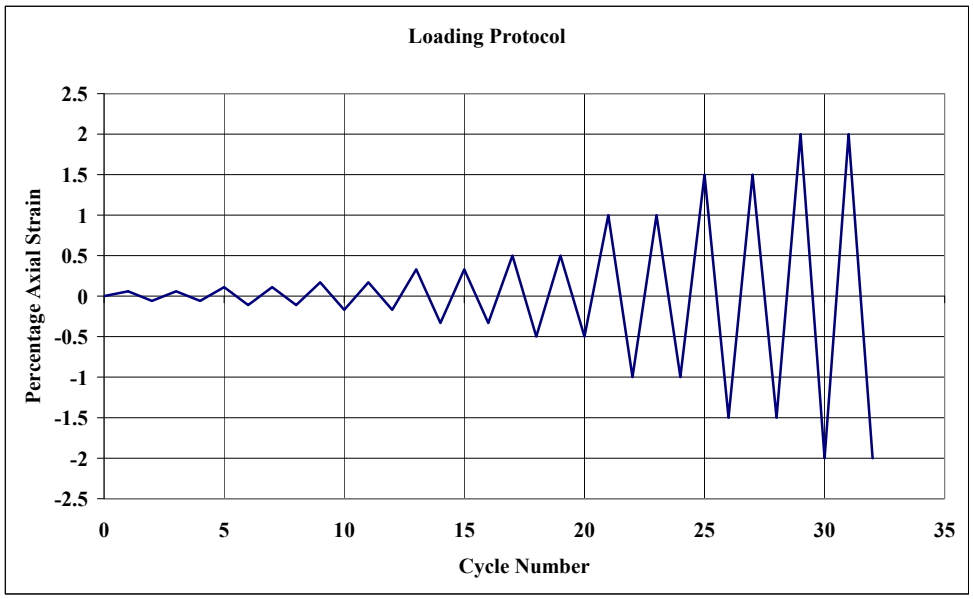

Figure 2.3 – Loading Protocol

2.3 Test Specimens

The testing program was developed by evolutionary changes made to the test specimens. Details of specimen dimensions are given in Table 2.1. The number of test specimen represents the order in which the specimen was tested. After each test was conducted, the author decided on the parameters that need further investigation and the necessary modifications for the following experiment. In order to help the readers easily to follow the thought process, first the general layout of the specimens is presented in this section. Later, details of each specimen are discussed in sections of the thesis which present the experimental findings.

All specimens had a rectangular yielding core segment (Fig. 2.4). Because of the limited screw jack capacity, the thickness of the core material used was limited to 5 mm. Depending on the aspect ratio, 40 mm, 60 mm, and 80 mm wide core segments were tested. The 40 x 5 mm core segments were obtained as flat bars. These were made of European S355 grade (En 10025, 1994) steel and the measured yield stress (F_y) and the ultimate stress (F_u) were 355 MPa and 510 MPa, respectively. All flat bars were from the same batch. Because no flat bars were available for larger widths, other core segments were produced from a plate. A 5 mm plate was cut using a precision controlled CNC machine to 60 mm and 80 mm widths. The plate material was made of European S275 grade (En 10025, 1994) steel and the measured yield stress (F_y) and ultimate stress (F_u) was 280 MPa and 420 MPa, respectively.

Two 120 mm long 40 by 5 mm cross section stiffening plates were fillet welded on both ends of the core segment to produce a cruciform nonyielding segment (Fig 2.4). Later the core segment cruciform ends were fillet welded to 10 mm thick plates which were used to fasten the specimen to the crossheads of the test setup. Four 20 mm diameter high strength European grade 8.8 bolts (BS 3692, 2001) were used to connect the specimen to any one of the crossheads. This kind of an attachment detail provides full fixity against rotation at both ends.

For all specimens the 900 mm long yielding core segment was wrapped with four layers of 0.05 mm thick polyethylene film which was secured by a tape. The polyethylene film functioned as a debonding material. For specimens 5 through 12, grease was also applied to the surface of the outer polyethylene film to help reduce the frictional forces. Width and thickness of the core segment were measured at five locations using a digital caliper which is accurate to 0.01 mm before the film was wrapped. Same measurements were conducted after testing to monitor the strain levels along the core segment.

Both the strong axis and the weak axis buckling of the steel core have to be prevented for satisfactory performance. The core segment was sandwiched between steel encasing members to prevent weak axis buckling. Filler plates having cross sectional dimensions of 20 mm by 5 mm were placed on both sides of the core segment to prevent strong axis buckling. Filler plates were continuous along the length of the member and there was a gap of 1 mm between the filler plate and the core segment. This gap allowed for the lateral expansion of the core segment in the longitudinal direction.

Rolled European channel sections were used as encasing members for the first six specimens while built-up shapes were used for the others. Encasing members and the filler plates that make up the buckling restraining mechanism were connected to each other either by welding or by bolting. For all specimens an 80 mm by 25 mm portion at both ends of the encasing members were removed to allow for the free elongation and shortening of the core segment.

2.4 Details of Test Specimens and Specimen Performance

General layout of the specimens was presented in the previous section. Specific details for each specimen and hysteretic response obtained through experimentation are presented in this section. The compression strength adjustment factor, β, and the strain hardening adjustment factor, ω, are calculated for each strain cycle beyond the yield and the values are presented in Tables 2.2 and 2.3.

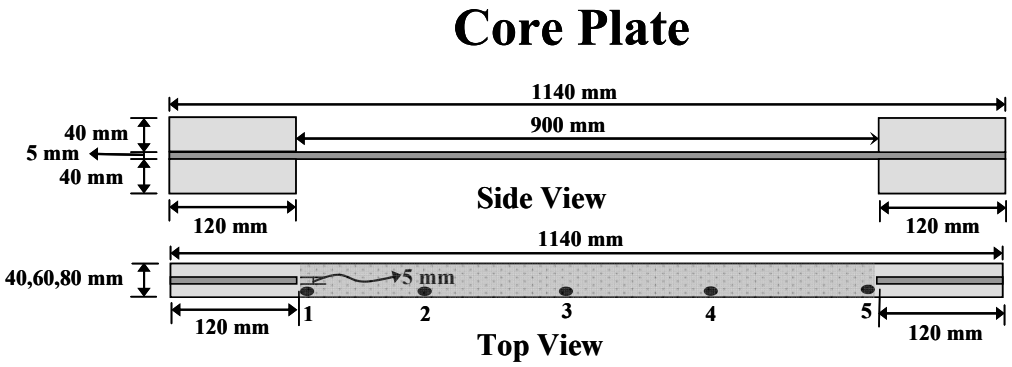

Figure 2.4 – Drawing of Typical Core Plate (Not to Scale)

Table 2.1 - Properties of Test Specimens

Specimen No	Core Plate			Encasing							Pcr/Py	Encasing Weight (kg)
	Dimension (mm)	Aspect Ratio	Fy (MPa)	Type	Section	Connection	Weld Type	Bolt Pretension	Attachment	Imperfection		
1	40x5	8:1	355	R	UPN 65	W	INT	-	F	N	21.85	15.44
2	40x5	8:1	355	R	UPN 65	W	CONT	-	F	N	21.85	15.44
3	40x5	8:1	355	R	UPN 120	B	-	S	F	N	56.37	28.06
4	40x5	8:1	355	R	UPN 120	B	-	H	F	N	56.37	28.06
5	40x5	8:1	355	R	UPN 120	B	-	H	T	Y	56.37	28.06
6	40x5	8:1	355	R	UPN 120	B	-	H	T	N	56.37	28.06
7	40x5	8:1	355	BU	60x6 - 25x25x2	W	INT	-	T	N	6.08	9.44
8	40x5	8:1	355	BU	80x5 - 50x5	B	-	H	T	N	4.71	10.84
9	60x5	12:1	280	BU	80x5 - 25x25x2	W	INT	-	T	N	4.74	10.06
10	80x5	16:1	280	BU	100x5 - 25x25x2	W	INT	-	T	N	3.16	11.62
11	60x5	12:1	280	BU	100x5 - 50x5	B	-	H	T	N	4.86	12.40
12	80x5	16:1	280	BU	120x5 - 50x5	B	-	H	T	N	3.29	13.98

R : Rolled BU : Built up W : Welded B : Bolted INT : Intermittent CONT : Continuous

S : Snug Tight H : Hand Tight F : Friction T : Tack Weld Y : Yes N : No

Pcr : Critical Buckling Load of Encasing Py : Yield Load of Core Brace

Table 2.2 - β Factors for Specimens

Specimen No	β Factors for Post Yield Strain Amplitudes				
	0.33 %	0.50 %	1.00 %	1.50 %	2.00 %
	β	β	β	β	β
1	1.059	1.048	1.059	1.013	0.909
2	1.032	1.089	1.139	1.163	1.217
3	1.076	1.090	1.149	1.202	1.257
4	1.042	1.054	1.153	1.237	1.352
5	1.006	1.054	1.070	1.077	1.139
6	1.011	1.038	1.064	1.075	1.094
7	1.088	1.084	1.131	1.166	1.201
8	1.000	1.042	1.059	1.067	1.089
9	1.024	1.041	1.071	1.090	1.111
10	1.021	1.021	1.056	1.070	1.085
11	1.028	1.020	1.047	1.068	1.081
12	1.045	1.024	1.043	1.056	1.046

Table 2.3 – ω Factors for Specimens

Specimen No	ω Factors for Post Yield Strain Amplitudes				
	0.33%	0.50%	1.00%	1.50%	2.00%
	ω	ω	ω	ω	ω
1	0.979	0.982	1.048	1.073	1.098
2	1.008	1.015	1.096	1.163	1.218
3	1.113	1.172	1.266	1.324	1.368
4	1.000	1.011	1.089	1.176	1.248
5	0.935	0.934	1.008	1.075	1.131
6	1.000	1.002	1.082	1.152	1.210
7	1.046	1.053	1.120	1.180	1.232
8	1.042	1.035	1.096	1.169	1.225
9	1.032	1.018	1.072	1.155	1.229
10	1.016	1.019	1.054	1.134	1.204
11	1.011	0.998	1.051	1.133	1.207
12	0.987	0.998	1.041	1.115	1.187

2.4.1 Specimen 1

UPN 65 channel sections were used as encasing members for Specimen 1 as shown in Fig. 2.5. The selection of this section was based on the required depth of the section. Filler plates and encasing members were welded to each other at large intervals in order to reduce the amount of friction produced by the compressive stresses formed during the cooling of welds. The intermittent welding detail is given in Fig. 2.5. In general 6 mm long welds were applied with 8 mm spacing. In this specimen, there was no attachment between the core segment and the buckling restraining mechanism. The vertical movement of the buckling restraining mechanism due to gravity was prevented by the frictional forces forming between the core and the encasing. Stiffening plates (Fig. 2.5) on both sides and at both ends of the specimen were welded to the channel sections to prevent local buckling of the core in this region.

Specimen 1 behaved well up to 1 percent strain (Fig. 2.6). For this strain value the difference between the maximum tensile and compressive loads reached to 5.9 percent. Minor load drops were observed during the first compressive excursion of the 1.5 percent strain cycle. These load drops were recovered as the strain was increased. This behavior can be attributed to the higher order buckling of the steel core in the weak axis. Although the decreases in loads were recovered, the global load displacement response had a negative slope after compressive strain reached to 1 percent. As a result, the maximum compressive load reached at 1.5 percent strain is smaller than the one reached at 1 percent strain.

A separation between the channel sections due to the bending of filler plates was observed during the second compressive excursion of the 1.5 percent compressive strain cycle. The specimen behaved in a similar way for the 2 percent strain cycle but this time the load drops due to higher order buckling were more severe. In addition, the tensile stiffness of the specimen reduced significantly due to straightening of the higher order buckled steel core. This specimen showed poor performance at higher strains due to the large spacing between the welds. When the testing was stopped, the mid-span opening between the two channel sections was 13 mm. A photo of the specimen after testing is given in Fig. 2.7.

Specimen 1

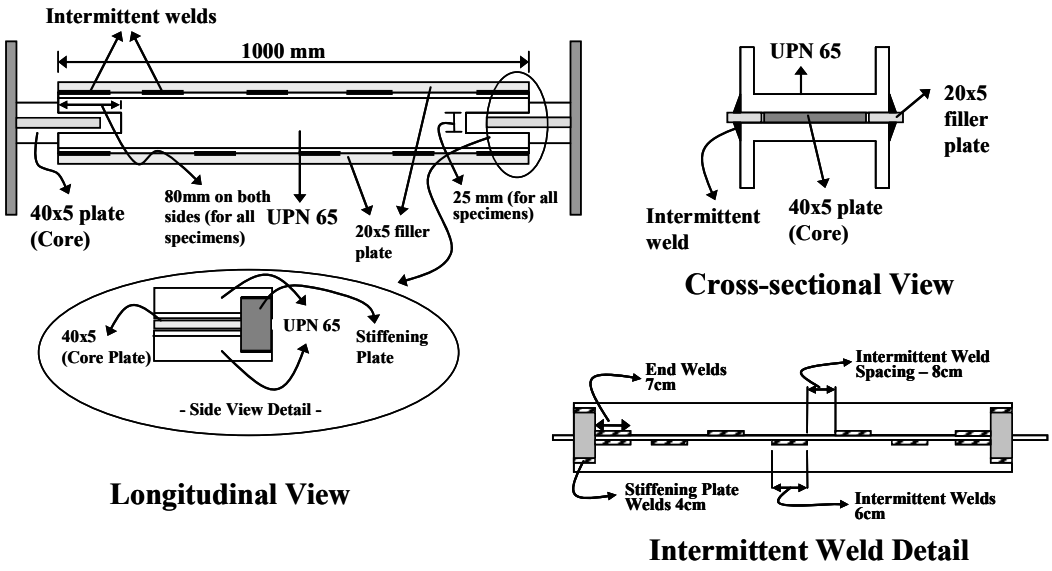

Figure 2.5 – Representative Drawing of Specimen 1 (Not to Scale)

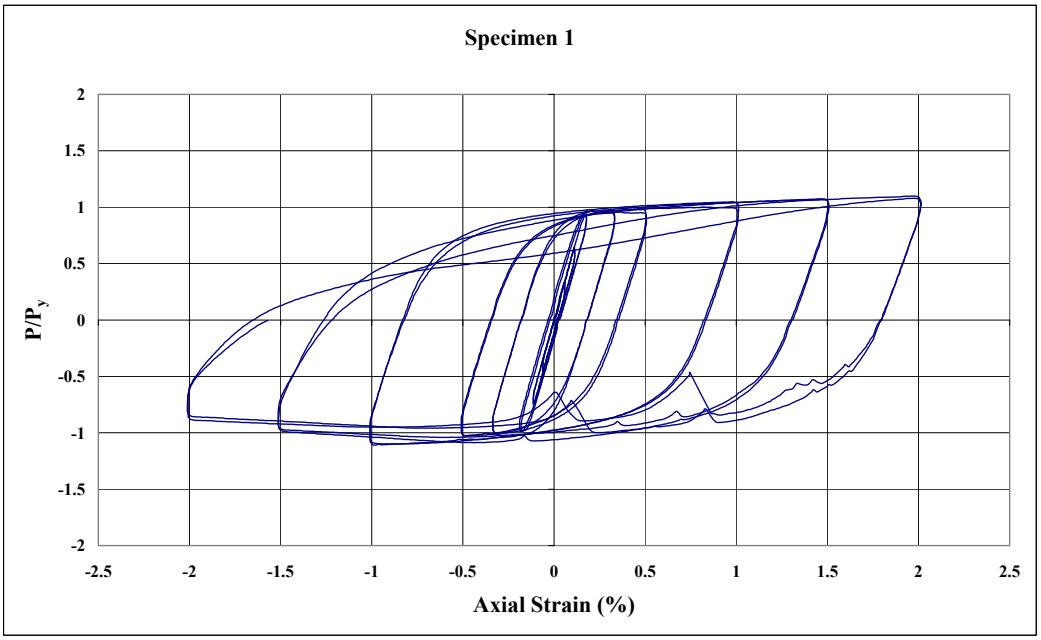

Figure 2.6 – Normalized Axial Load vs. Axial Strain for Specimen 1

Figure 2.7 – Photo of Specimen 1 after Testing

2.4.2 Specimen 2

Specimen 2 was identical to Specimen 1 except that the filler plates and the channel sections were connected using continuous fillet welds (Fig. 2.8). Specimen 2 showed stable hysteretic behavior (Fig. 2.9). The difference between maximum tensile and compressive loads reached to 21.7 percent. Vertical movement of the encasing was not observed during the experiment. Accordingly the cooling of welds produces a clamping force that results in the formation of frictional resistance between the core and the encasing.

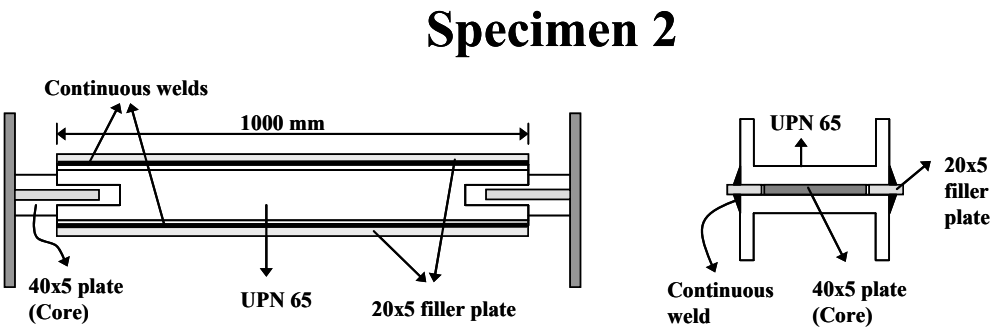

Figure 2.8 – Representative Drawing of Specimen 2 (Not to Scale)

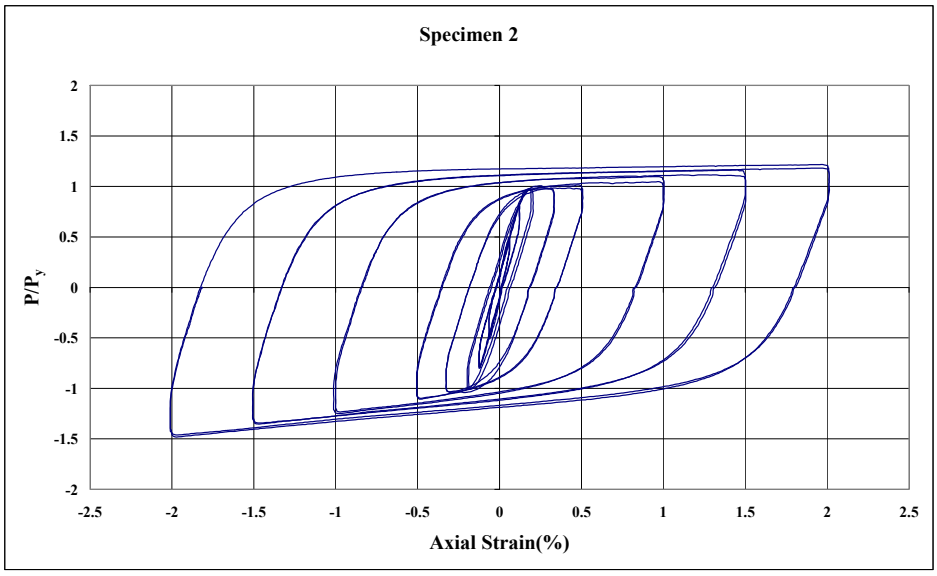

Figure 2.9 - Normalized Axial Load vs. Axial Strain for Specimen 2

2.4.3 Specimen 3

UPN 120 channel sections were used as encasing members for Specimen 3 as shown in Fig. 2.10. As opposed to the first two specimens, this one had bolted connections. After observing poor performance of Specimen 1 due to largely spaced welds, it was decided to closely space the bolts for Specimen 3. A total of 40 grade 8.8 high strength bolts with 10 mm diameter (M10) were used to connect the filler plates and the channel sections. As shown in Fig. 2.10 bolts ran through the webs of the channels and the filler plates. A deep channel with 120 mm web height was used to restrain the core using this arrangement. Bolt holes were also drilled to 10 mm diameter. Spacing between the bolt holes was 50 mm center-to-center.

In this specimen bolts were tightened to prevent the vertical movement of the buckling restraining mechanism. First the bolts were hand tightened and then they were brought to snug-tight condition by applying three quarter turns using a spud wrench.

Specimen 3 showed stable hysteretic behavior (Fig. 2.11). The difference between maximum tensile and compressive loads reached to 25.7 percent. As compared to Specimen 2, this specimen reached to higher tensile and compressive loads. This is attributable to the large amounts of friction developing at the interfaces due to the tightening of the bolts. For this specimen no vertical movement of the encasing was observed.

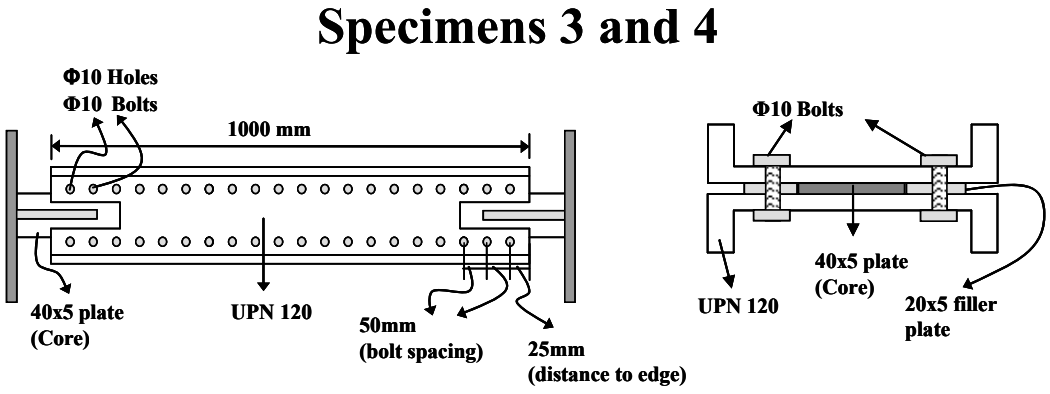

Figure 2.10 – Representative Drawing of Specimens 3 and 4 (Not to Scale)

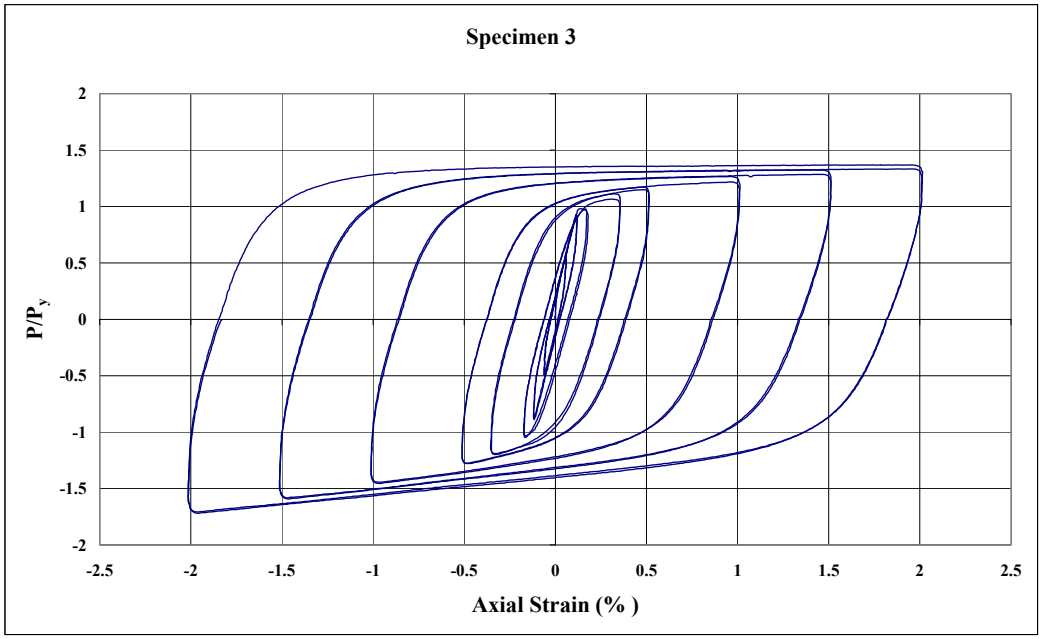

Figure 2.11 - Normalized Axial Load vs. Axial Strain for Specimen 3

2.4.4 Specimen 4

Configuration of Specimen 4 was identical to the one of Specimen 3 (Fig. 2.10). In this specimen the effect of bolt pretension was studied. Only one row of bolts at the center of the specimen was tightened to snug-tight condition to prevent the vertical movement of the encasing. All other bolts were hand tightened.

Specimen 4 showed stable hysteretic behavior (Fig. 2.12). However, slipping of the encasing was observed during the last cycles. During the second cycle of the 2 percent strain, the encasing completely slipped and came into contact with the cruciform end of the core segment. This resulted in the transfer of forces to the buckling restraining segment. Therefore, for this cycle the difference between maximum tensile and compressive loads reached to 35.2 percent. This difference was only 21 percent for the first cycle of the 2 percent strain. When compared with Specimen 3, this specimen except the very last cycle reached to lower tensile and compressive loads. This is due to the reduced amount of friction created by loose bolts.

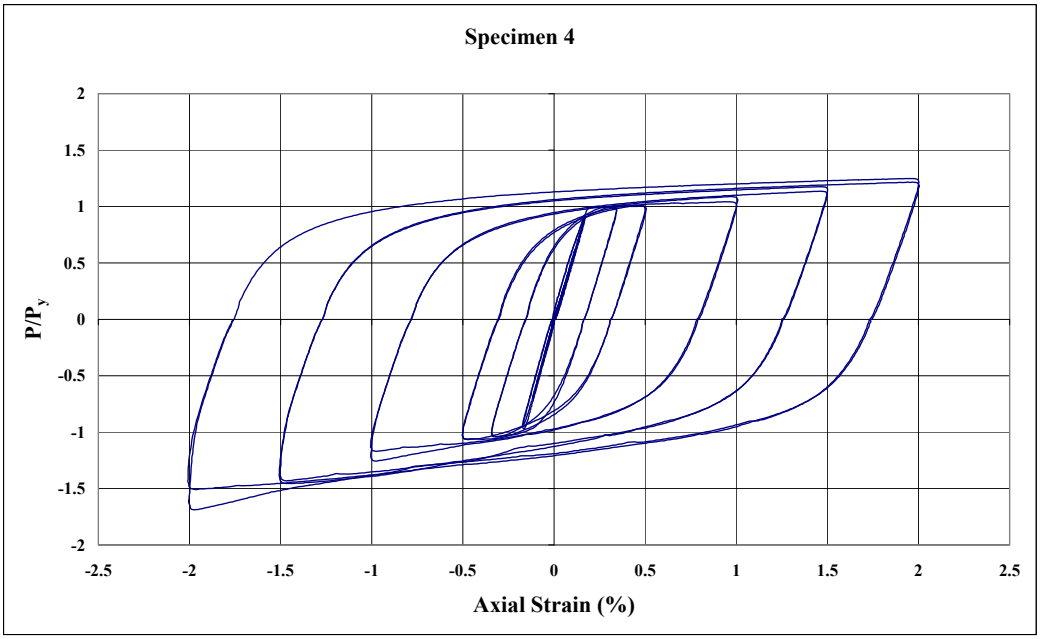

Figure 2.12 - Normalized Axial Load vs. Axial Strain for Specimen 4

2.4.5 Specimen 5

Configuration of Specimen 5 was identical to the one of Specimen 4. In order to prevent slip, core segment was tack welded to one of the channel sections at the midspan. Tack welds were deposited between the filler plates and the core segment. Same encasing member used for Specimen 4 was used for this specimen. Same grade 8 mm diameter bolts were used rather than 10 mm diameter bolts. All bolts were hand tightened. It was observed that the encasing members did not perfectly fit to the core segment after the encasing member was fastened (Fig. 2.13). Basically due to the uneven cooling of the tack welds there was a gap between the core plate and the channel section. When both channel sections were fastened to the core segment there was a 1 mm side opening at the mid-length between the channels. At this point it was realized that this kind of an imperfection may as well be present in a buckling restrained brace that will be constructed for a real application in the future. Therefore, in order to observe the consequences of having such imperfections it was decided to test this specimen without any modifications.

Specimen 5 showed stable hysteretic behavior. However, due to the presence of imperfections local buckling of the core segment in the weak direction was observed. Local buckles resulted in load drops as shown in Fig. 2.14. Although load values decreased due to local buckling, increase in strains resulted in the recovery of these

loads. Therefore, no significant strength degradation was observed. The difference between maximum tensile and compressive loads reached to 13.9 percent. Tack welding the core plate to one of the channels prevented vertical slip of the encasing and did not have an adverse effect on the global behavior. Consequently, for specimens tested after Specimen 5 this kind of an attachment detail was used.

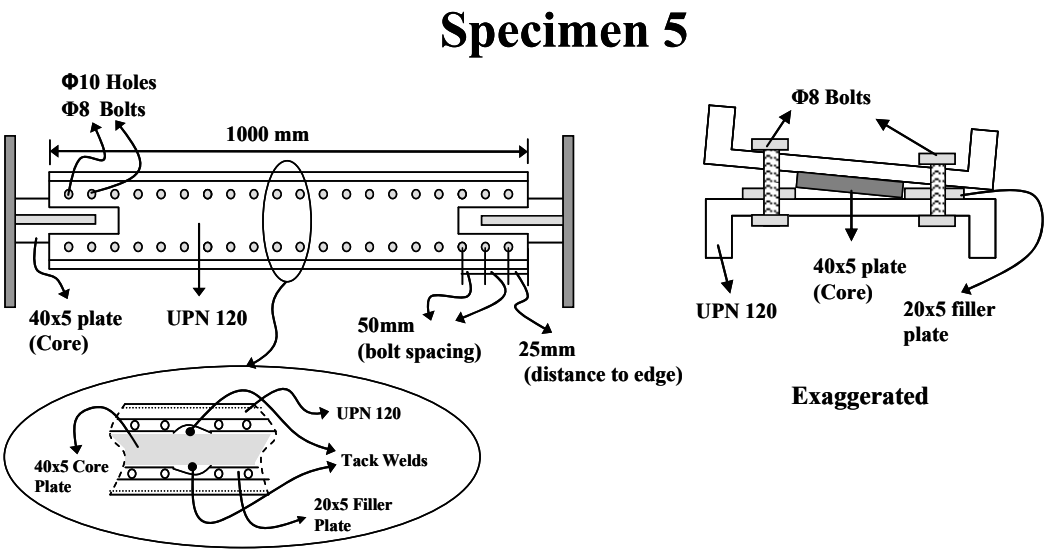

Figure 2.13 – Representative Drawing of Specimen 5 (Not to Scale)

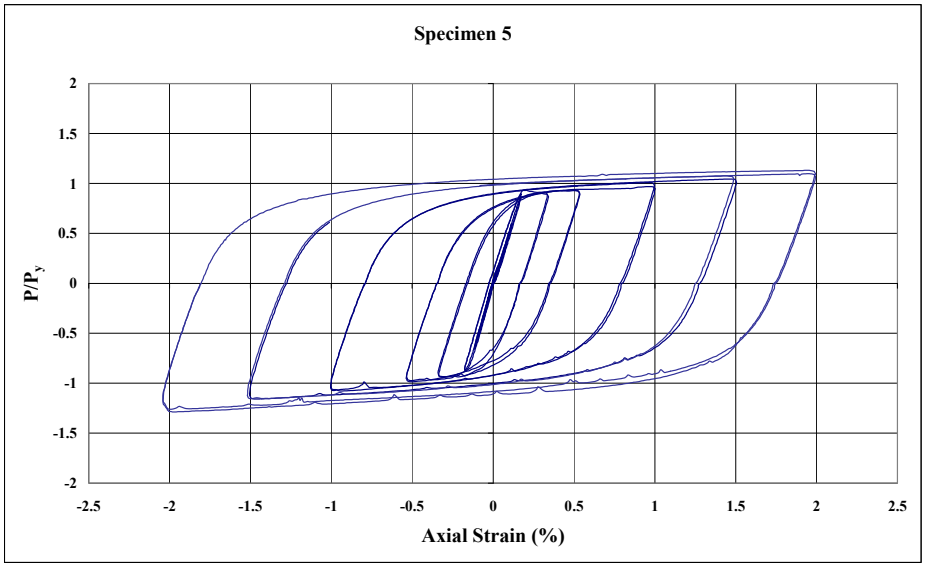

Figure 2.14 - Normalized Axial Load vs. Axial Strain for Specimen 5

2.4.6 Specimen 6

Specimen 6 was identical to Specimen 5 (Fig 2.15). For this specimen a different type of tack weld detail was used to reduce the amount of imperfection due to cooling of welds. Basically cross sectional areas of filler plates were reduced at the mid-span as shown in Fig. 2.16. This reduction enabled to deposit the tack welds with more precision. In the welding process the core plate was first secured to the channel encasing by making use of C-clips. Then tack welds were deposited to both sides of the core plate and allowed to cool. After cooling of the welds the C-clips were removed and the buckling restraining mechanism was fastened using high strength bolts.

Specimen 6 showed stable hysteretic behavior (Fig. 2.17). Unlike Specimen 5 no load drops were observed in any of the compression excursions. The difference between maximum tensile and compressive loads reached to 9.4 percent.

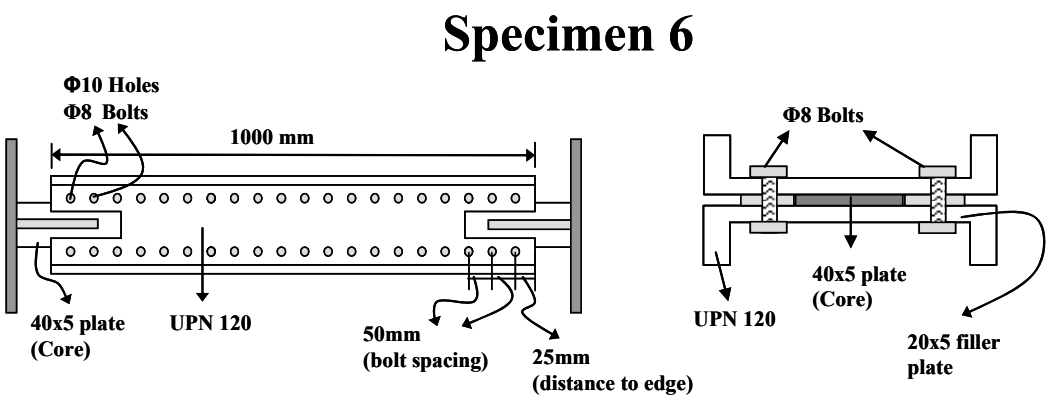

Figure 2.15 – Representative Drawing of Specimen 6 (Not to Scale)

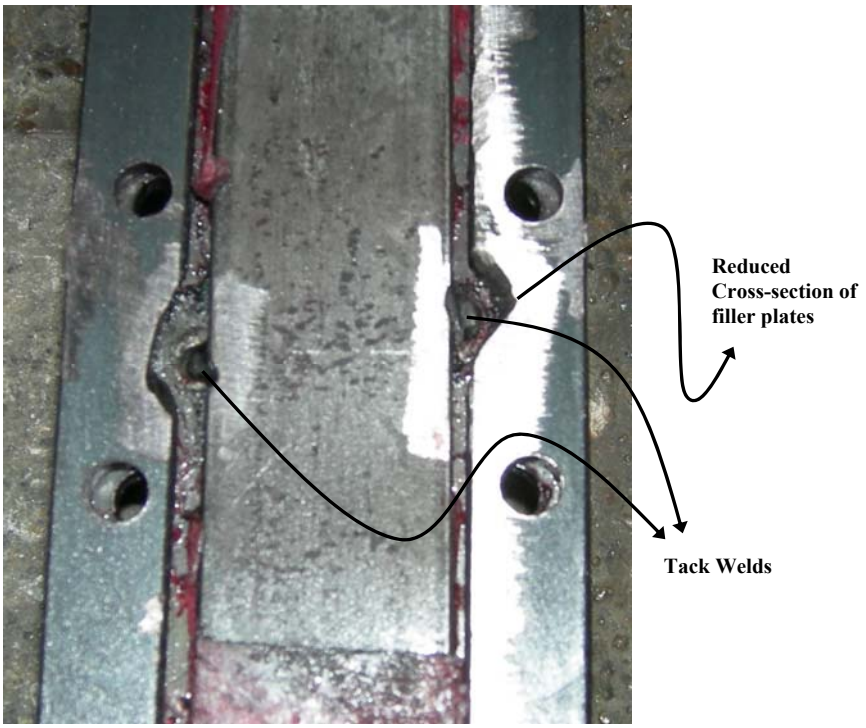

Figure 2.16 – Photo of Tack Weld Attachment for Encasing Member

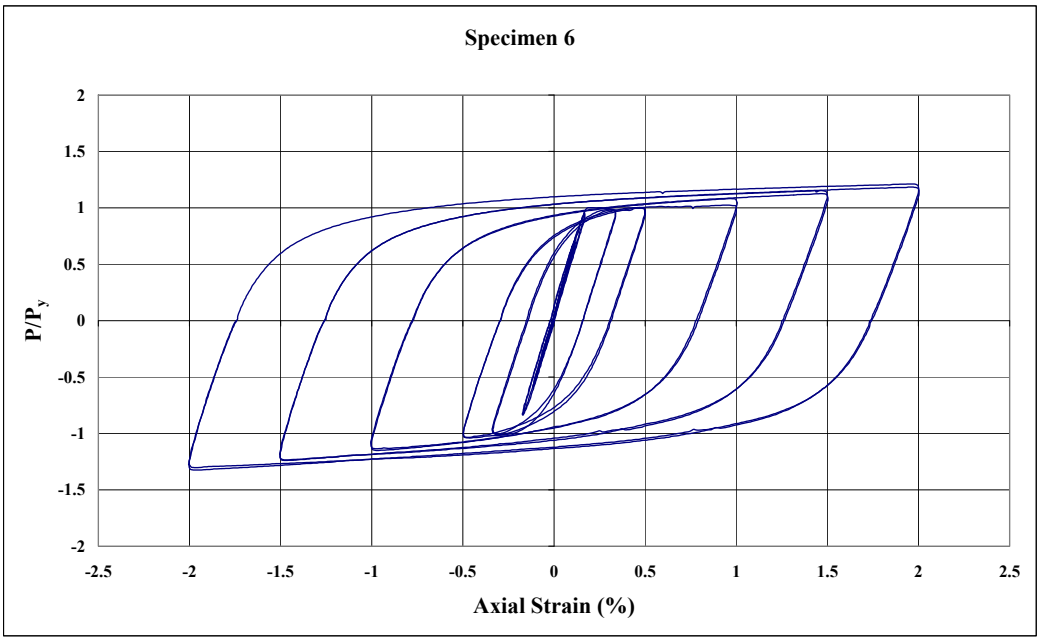

Figure 2.17 – Normalized Axial Load vs. Axial Strain for Specimen 6

2.4.7 Specimen 7

A welded buckling restraining mechanism with built-up sections was used as encasing for Specimen 7 (Fig. 2.18). Rolled shapes were used for encasing in the previous specimens. Built-up sections were used for the rest of the specimens in order to develop buckling restrained braces with lighter encasing. The built-up section for this specimen was formed by welding a 25x25x2 mm box section to a 60x6 mm flat bar. The critical buckling load of the buckling restraining mechanism was 6.1 times the yield load of the steel core. Previous research (Watanabe et al., 1988) has demonstrated that the buckling load should be at least 1.5 times the yield load of the core segment. Buckling restraining mechanism was formed by intermittent welding of the two built-up sections. Intermittent welds at every 50 mm were used to reduce the amount of clamping force produced during the cooling of welds.

Specimen 7 showed stable hysteretic behavior (Fig. 2.19). The difference between maximum tensile and compressive loads reached to 20.1 percent.

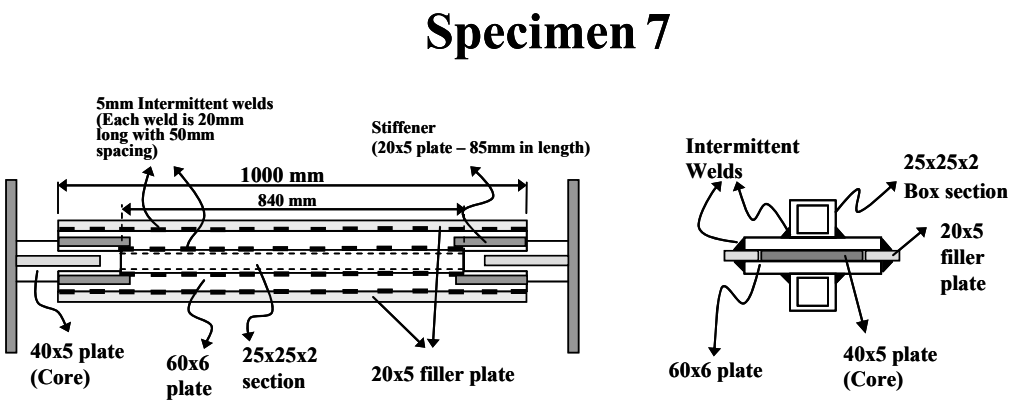

Figure 2.18 – Representative Drawing of Specimen 7 (Not to Scale)

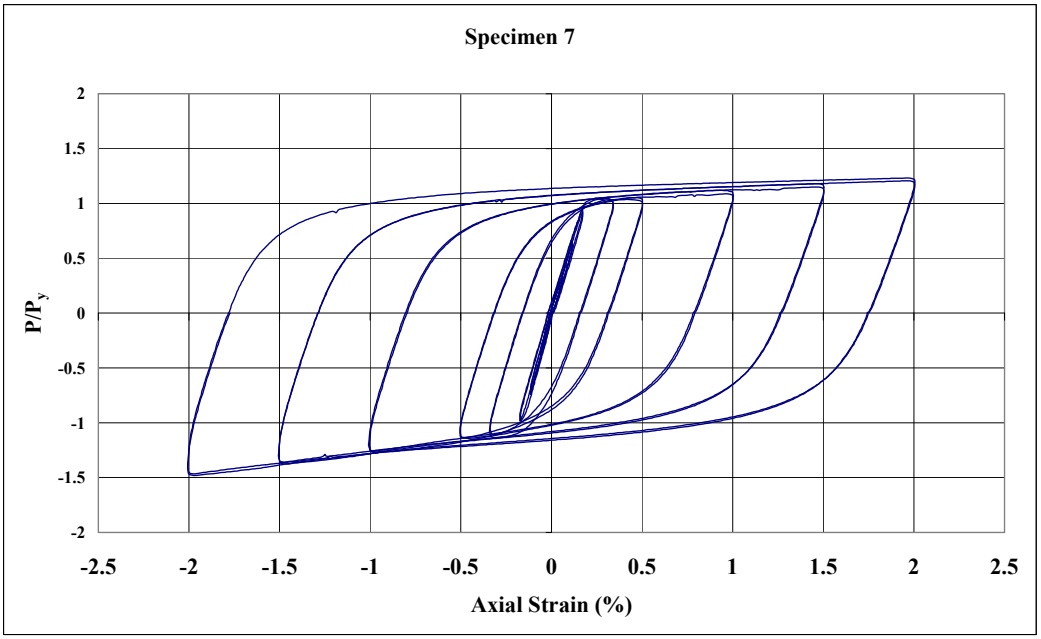

Figure 2.19 – Normalized Axial Load vs. Axial Strain for Specimen 7

2.4.8 Specimen 8

A bolted buckling restraining mechanism with built-up sections was used as encasing for Specimen 8. The built-up section for this specimen had a T-shape and was formed by welding 80x5 mm and 50x5 mm flat bars (Fig. 2.20). The critical buckling load of the buckling restraining mechanism was 4.7 times the yield load of the steel core. In finding the buckling load of the restraining mechanism it was assumed that both built-up sections bend independently. Grade 8.8 high strength bolts with 8 mm diameter were used to connect the built-up sections. Bolts were placed at 50 mm intervals.

Specimen 8 showed stable hysteretic behavior (Fig. 2.21). The difference between maximum tensile and compressive loads reached to 8.9 percent.

Specimen 8

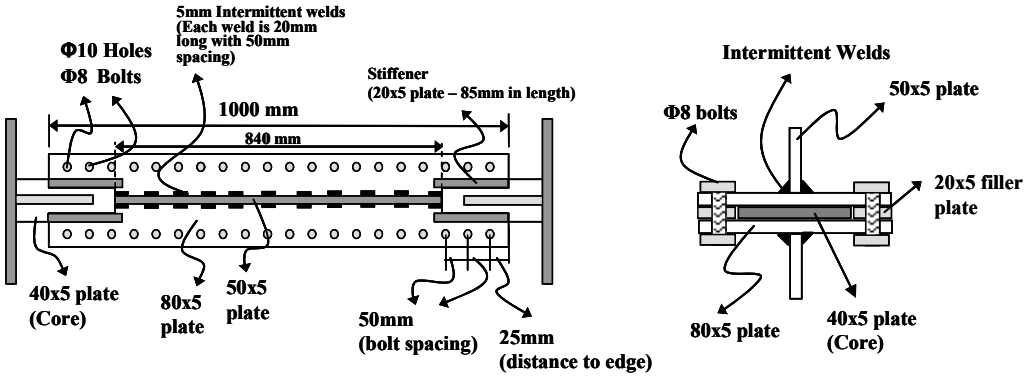

Figure 2.20 – Representative Drawing of Specimen 8 (Not to Scale)

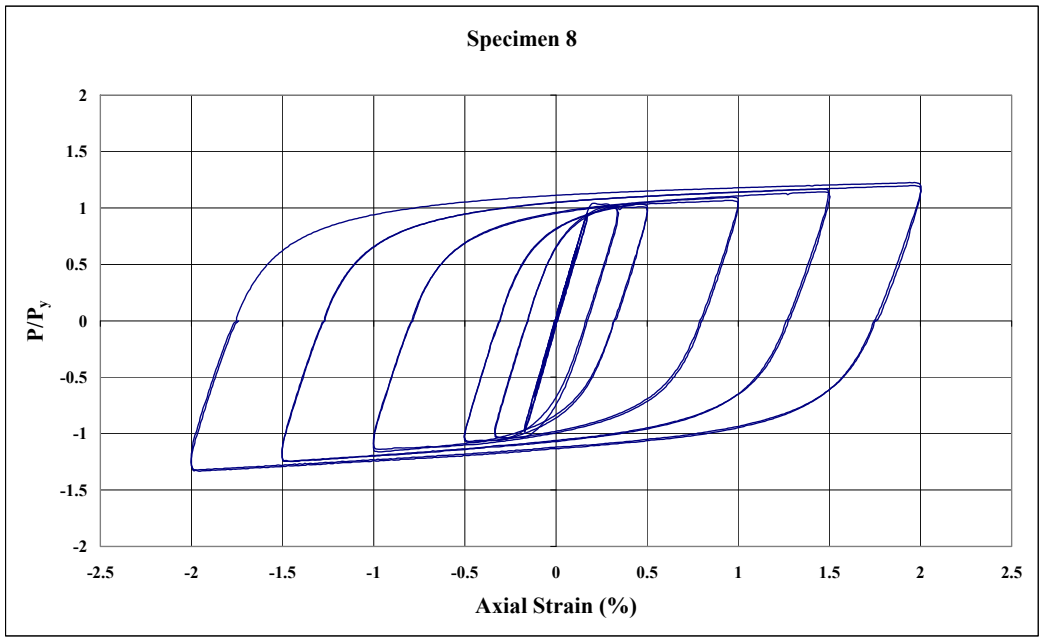

Figure 2.21 – Normalized Axial Load vs. Axial Strain for Specimen 8

2.4.9 Specimen 9

The aspect ratio of the core plate was 8 for the previous experiments. Core segments with higher aspect ratios were experimented for the rest of the specimens. A 60x5 mm core with an aspect ratio of 12 was used for Specimen 9 (Fig. 2.22). The buckling restraining mechanism consisted of built-up sections intermittently welded to each other. The built-up section consists of an 80x5 mm flat bar connected to a 25x25x2 box section.

Specimen 9 showed stable hysteretic behavior (Fig. 2.23). The difference between maximum tensile and compressive loads reached to 11.1 percent.

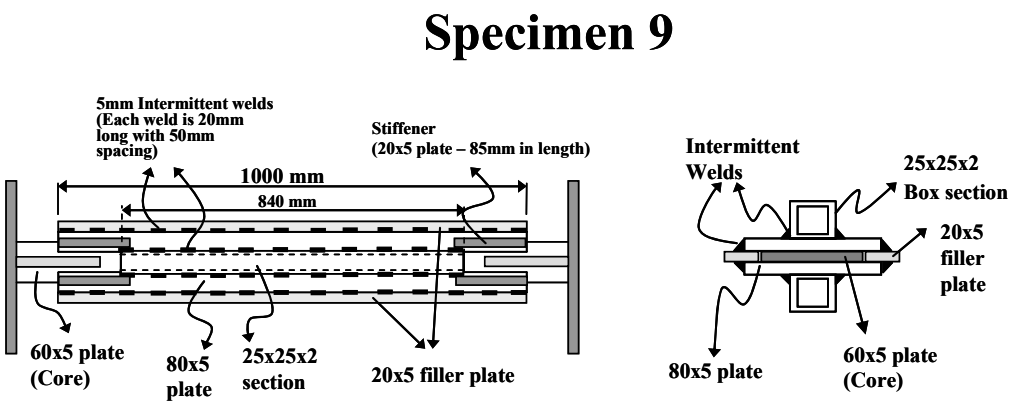

Figure 2.22 – Representative Drawing of Specimen 9 (Not to Scale)

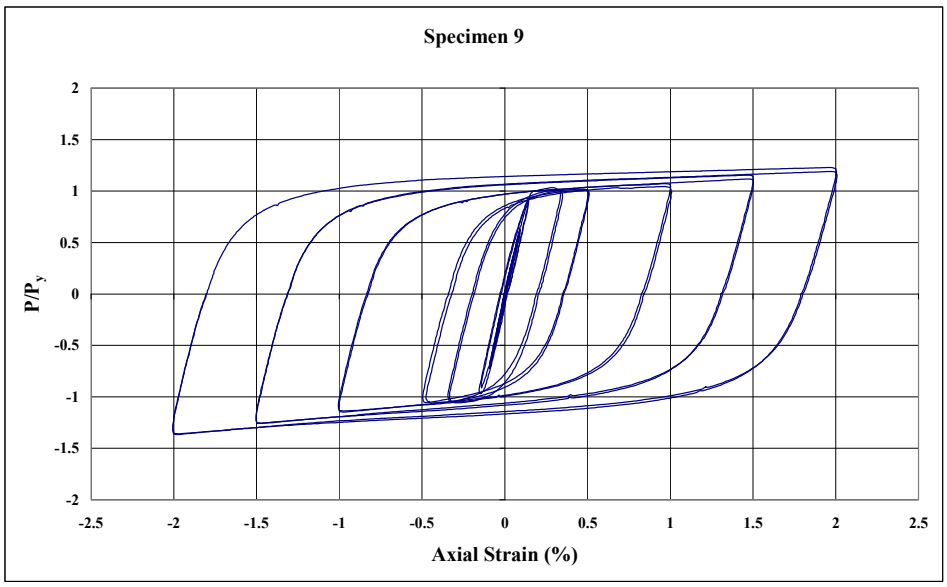

Figure 2.23 – Normalized Axial Load vs. Axial Strain for Specimen 9

2.4.10 Specimen 10

An 80x5 mm core with an aspect ratio of 16 was used for Specimen 10. Aspect ratios on this order have not been significantly studied in the past. This specimen had built-up sections that are intermittently welded together to form a buckling restraining mechanism. The built-up section consists of a 100x5 mm flat bar connected to a 25x25x2 box section (Fig. 2.24).

Specimen 10 showed stable hysteretic behavior (Fig. 2.25). The difference between maximum tensile and compressive loads reached to 8.5 percent.

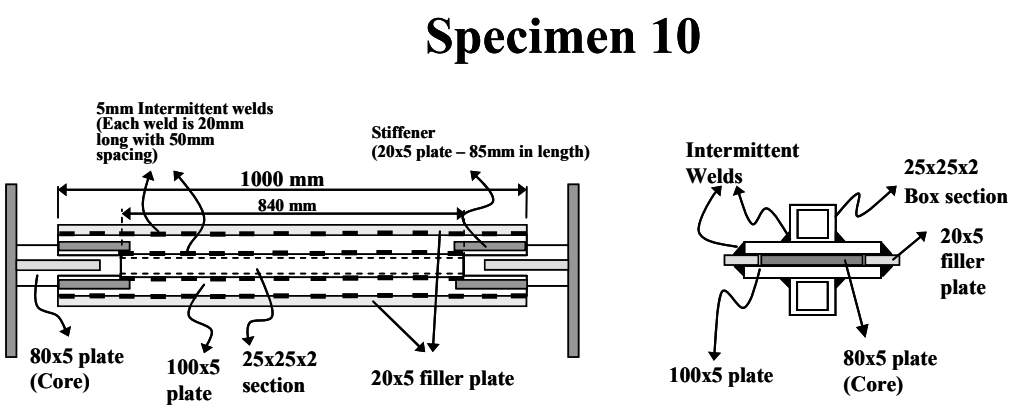

Figure 2.24 – Representative Drawing of Specimen 10 (Not to Scale)

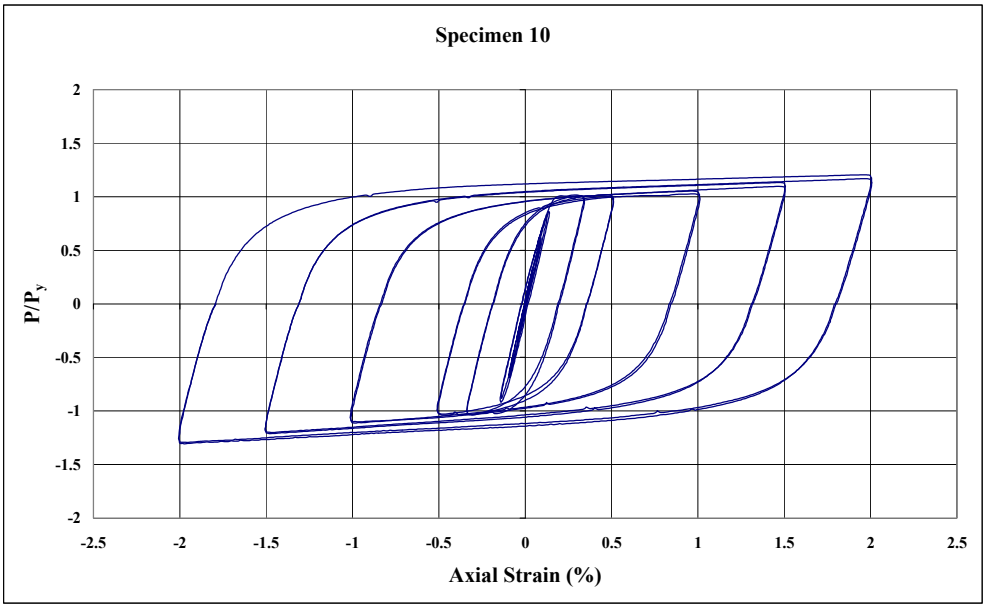

Figure 2.25 – Normalized Axial Load vs. Axial Strain for Specimen 10

2.4.11 Specimen 11

The core segment of this specimen was identical to the one of Specimen 9. This specimen had a bolted buckling restraining mechanism instead of a welded one (Fig. 2.26). The built-up encasing section consists of a T-shape formed by welding 100x5 mm and 50x5 mm plates. Specimen 11 showed stable hysteretic behavior. The difference between maximum tensile and compressive loads reached to 8.1 percent.

For specimen 7 additional cycles at 2 percent strain were applied after the original loading sequence was finished. These additional cycles resulted in a cumulative ductility of 600 times the yield deformation. Behavior of this specimen with additional loading cycles is given in Fig. 2.27. At the 7th additional cycle minor load drops under compressive loading was observed. These drops, however, did not cause any detriment in the overall behavior. These load drops were indications of local buckles due to high amount of cumulative inelastic strains.

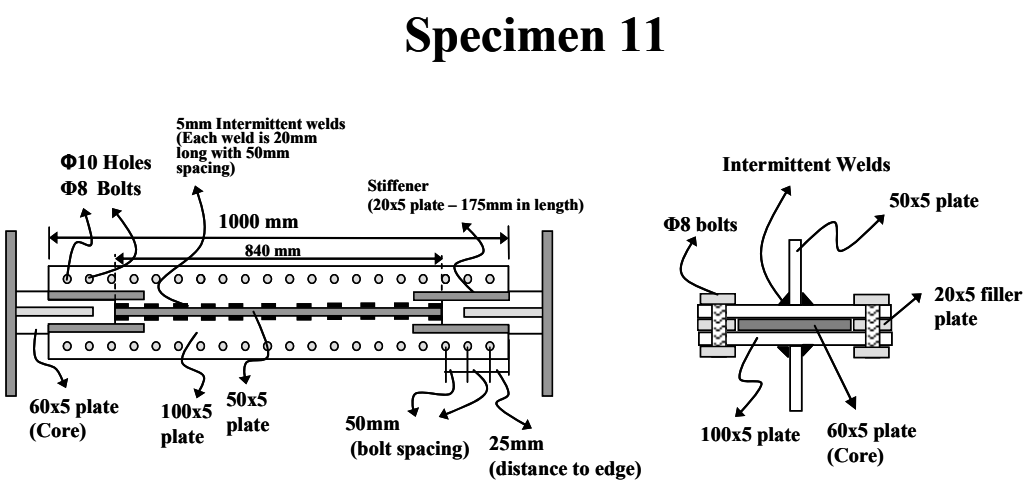

Figure 2.26 – Representative Drawing of Specimen 11 (Not to Scale)

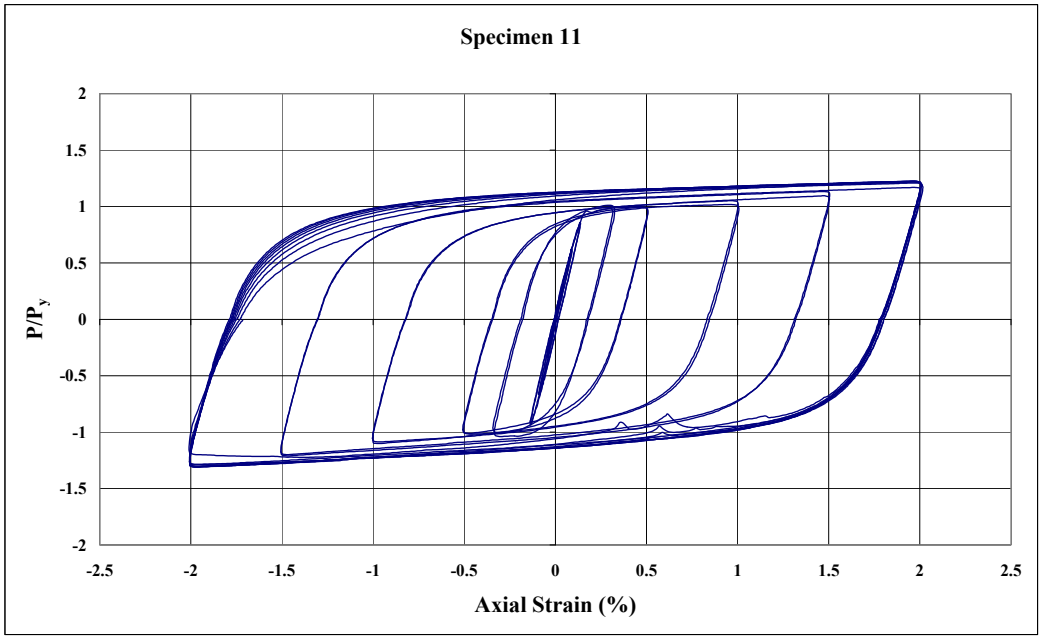

Figure 2.27 – Normalized Axial Load vs. Axial Strain for Specimen 11

2.4.12 Specimen 12

Specimen 12 had a core segment with an aspect ratio of 16. The buckling restraining had bolted connections like Specimen 11. The built-up encasing consists of a T-shape formed by welding 120x5 mm and 50x5 mm plates (Fig. 2.28). Specimen 12 showed stable hysteretic behavior (Fig. 2.29). The difference between maximum tensile and compressive loads reached to 4.6 percent.

Like Specimen 11 additional cycles at 2 percent strain were applied to this one. During the compressive excursion of the first additional cycle minor load drops were observed. In the following compressive excursion the load drops were even more significant. It was observed that the core brace experienced significant local buckling at one end as shown in Fig. 2.30. A total of three additional cycles were applied to this specimen and in all of these cycles the maximum amount of compressive force reduced. Testing had to be stopped due to the local buckle formed at the core segment. The encasing members should have stiffeners at the ends due to the large aspect ratio of the core plate. For this specimen longitudinal stiffeners were placed at the ends as shown in Fig. 2.28. However, there were no transverse stiffeners to prevent local bending of the encasing. Placing transverse stiffeners can be considered an option in future studies to increase the amount of cumulative ductility that high aspect ratio core plates sustain. This specimen endured a cumulative ductility of 450 times the yield deformation.

Specimen 12

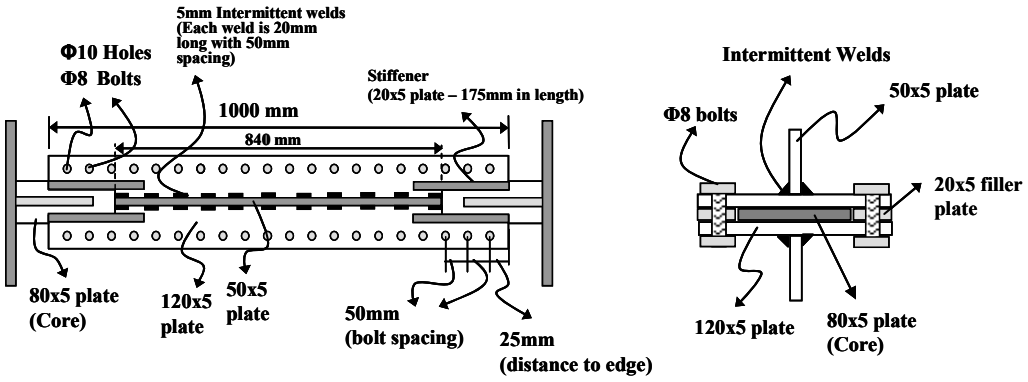

Figure 2.28 – Representative Drawing of Specimen 12 (Not to Scale)

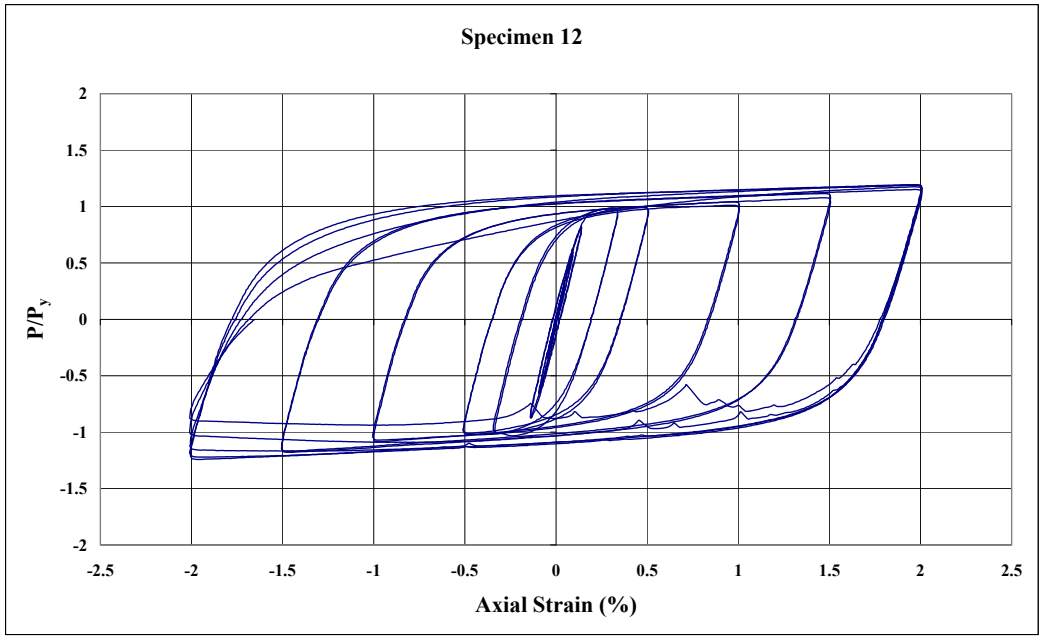

Figure 2.29 – Normalized Axial Load vs. Axial Strain for Specimen 12

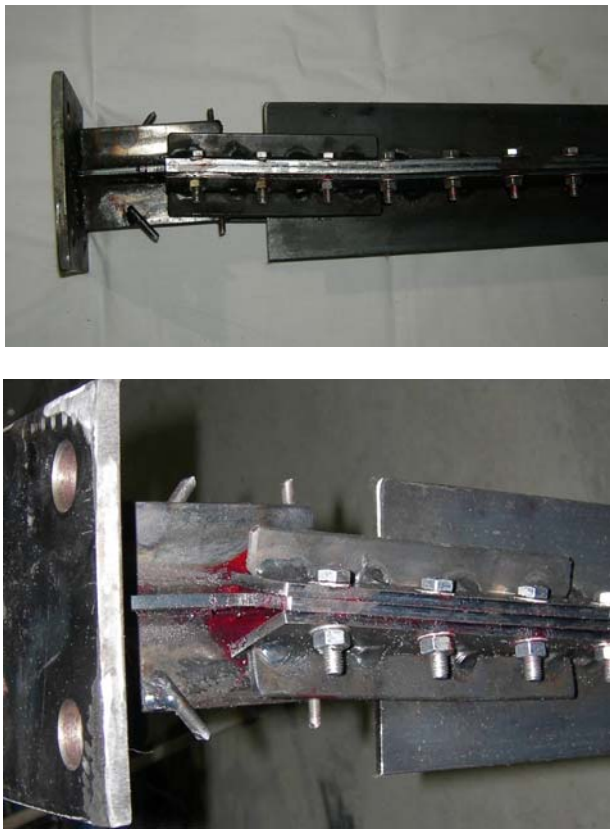

Figure 2.30 – Photos of Specimen 12 after Testing

2.5 Evaluation of Test Results

All specimens except the first specimen showed satisfactory performance. Apart from the global load-displacement response several other factors such as the adjustment factors, initial stiffness, yielding and buckling patterns are of interest. The following sections present details of the findings from experiments.

2.5.1 Compression Strength and Strain Hardening Adjustment Factors

As mentioned in section 2.4, the β and ω factors are tabulated in Tables 2.2 and 2.3. Values are given for axial strain values of 0.33, 0.50, 1.00, 1.50, and 2.00 percent. In general, there is an increase in the strain hardening adjustment factor (ω) with an increase in the strain amplitude. This is natural because of the cyclic strain hardening that takes place. The ω factor is influenced highly by the material properties and is also dependent on the amount of friction at the interface. A fair assessment of ω factors can be performed by grouping the specimens with the same material properties. Specimens 1 through 8 were from the same batch and the remaining ones were from another batch.

Regardless of the type of material used, the strain hardening factors were close to 1.2 for 2 percent axial strain. For Specimen 3, this value reached to 1.37, and this is an indication of the friction that is present due to the tightening of the bolts.

The compression strength adjustment factor is also influenced by the amount of friction and with the degree of lateral restraint. For welded specimens the β factor is greater when compared with the bolted specimens. This is due to the large clamping forces that are created during the cooling of welds. On the contrary, a similar behavior can be achieved if the bolts are significantly tightened as in the case of Specimen 3. Specimen 4 is the only case where the β factor is larger than 1.3. In this case, however, slipping of the encasing at later cycles caused it to carry some axial load which in turn modified the balance between load levels in tension and compression.

2.5.2 Initial Stiffness

Initial stiffness measurements of the specimens are useful in understanding the amount of friction transfer at the core-to-encasing interface. The stiffness values were calculated at one-third and two-thirds of the yield displacement and were normalized by the theoretical stiffness values. The normalized secant stiffness at one-third and two-thirds of the yield displacement are tabulated in Table 2.4 for tension and compression. All specimens were subjected to tensile loading first. The tension stiffness at the first cycle is usually higher than the stiffness at later cycles. The amount of friction is more influential on the initial cycles when compared with the later cycles. All cases except a few had normalized stiffness values close to unity. For Specimens 2 and 3 excessive stiffness values were observed. These are because of the continuous welding and significant amount of bolt tightening.

Table 2.4 – Initial Secant Stiffness Values

Normalized Tension and Compression Stiffness Values for $\Delta_y/3$ and $2*\Delta_y/3$ Cycles				
Specimen No	**Tension Stiffness**		**Compression Stiffness**	
	$\Delta_y/3$ Cycle	**$2*\Delta_y/3$ Cycle**	**$\Delta_y/3$ Cycle**	**$2*\Delta_y/3$ Cycle**
1	1.04	1.08	1.04	1.05
2	1.55	1.27	1.06	1.05
3	1.77	1.20	1.17	1.13
4	0.92	1.11	0.90	1.07
5	0.89	1.03	0.90	0.99
6	1.14	0.93	1.02	0.95
7	1.06	1.11	0.96	1.10
8	1.06	1.07	0.98	1.02
9	0.99	1.04	0.93	1.02
10	1.02	1.05	0.94	0.99
11	1.07	1.03	0.94	0.96
12	0.94	1.01	0.87	0.90

2.5.3 Yielding and Buckling Patterns

Uniform yielding along the length of the core segment is desired for a satisfactory performance in a BRB. Non-uniform straining can be due to the presence of frictional resistance on the core segment. There can be large local strains if the presence of frictional resistance is significant. These large strains usually trigger local buckling which leads to low cycle fatigue. In order to understand the variation of strains along the length, width and thickness measurements of the core plate were taken before and after each experiment. The change in cross sectional dimensions was measured at five locations that are shown in Fig. 2.4. Basically, measurements were taken at the ends, at the center and at quarter points. The change in width and thickness at these five locations are tabulated in Table 2.5. No measurements were taken for Specimen 1 due to its poor performance.

Table 2.5 – Percentage Strain Values for Width and Thickness of Specimens

Point Number	Specimen 1		Specimen 2		Specimen 3		Specimen 4		Specimen 5		Specimen 6	
	b (%)	t (%)	b (%)	t (%)	b (%)	t (%)	b (%)	t (%)	b (%)	t (%)	b (%)	t (%)
1	NA	NA	3.09	3.05	4.76	4.31	4.63	8.91	1.69	2.12	1.41	1.16
2	NA	NA	-0.15	0.00	0.00	-1.75	1.37	3.70	0.70	1.75	1.20	0.20
3	NA	NA	0.00	0.78	0.18	1.56	-0.20	-0.38	0.70	2.30	0.70	1.17
4	NA	NA	0.52	2.91	1.10	1.16	-1.02	0.19	0.08	2.10	0.45	0.20
5	NA	NA	3.71	4.85	5.15	5.25	0.95	1.54	1.35	1.73	1.35	0.78
Point Number	**Specimen 7**		**Specimen 8**		**Specimen 9**		**Specimen 10**		**Specimen 11**		**Specimen 12**	
	b (%)	t (%)	b (%)	t (%)	b (%)	t (%)	b (%)	t (%)	b (%)	t (%)	b (%)	t (%)
1	0.88	0.20	0.93	0.75	1.47	1.18	0.83	-0.39	NA	NA	-0.98	-0.20
2	0.85	-0.58	0.63	1.33	1.09	1.19	0.74	-0.78	-0.42	0.99	-1.05	-1.79
3	0.43	0.97	0.67	1.14	0.42	0.40	0.30	0.20	-0.70	-0.79	-1.00	-0.40
4	1.00	1.94	0.80	1.72	0.89	0.80	0.59	0.79	-0.02	1.40	NA	NA
5	1.18	1.54	1.12	0.95	1.24	2.21	NA	NA	1.68	2.80	NA	NA

b : Width t : Thickness

Values in Table 2.5 reveal that for specimens 2 and 3 the strain distribution along the length is non-uniform. Strains are more localized at the ends. These specimens had continuous welds or snug-tight bolted attachments. Non-uniform straining was also observed for Specimen 4. Measurements for this specimen are not reliable to draw firm conclusions because of the encasing slip that took place during loading.

For the remaining specimens axial strain values tend to be more uniform. Note that for some cases no measurements were taken because of a local buckle forming at the region of interest. Based on the strain observations it can be concluded that for specimens with intermittent weld or hand tight bolted attachments provide a uniform axial strain variation.

Buckling patterns of specimens were also investigated after each test. Some representative buckled configurations are given in Fig. 2.31. In general all specimens experienced strong axis global buckling. For some specimens with bolted attachments local buckles were also observed. These local buckles are usually located close the ends of the specimens.

SPECIMEN 2

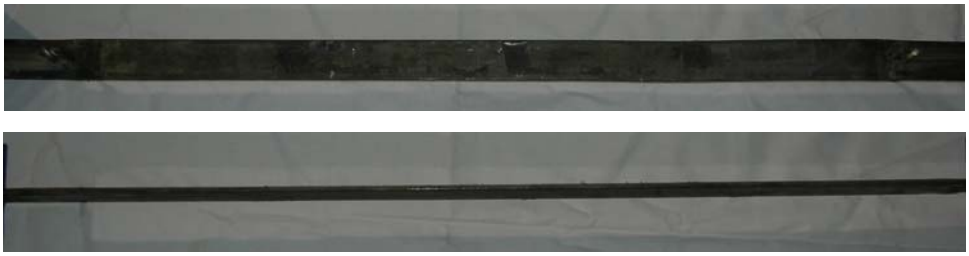

SPECIMEN 3

SPECIMEN 4

SPECIMEN 5

Figure 2.31 – Buckling Patterns of Specimens

SPECIMEN 6

SPECIMEN 7

SPECIMEN 8

SPECIMEN 9

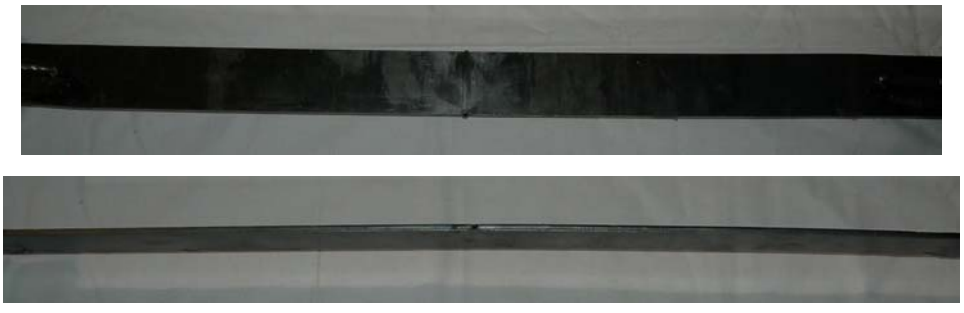

Figure 2.31 (continued) – Buckling Patterns of Specimens

SPECIMEN 10

SPECIMEN 11

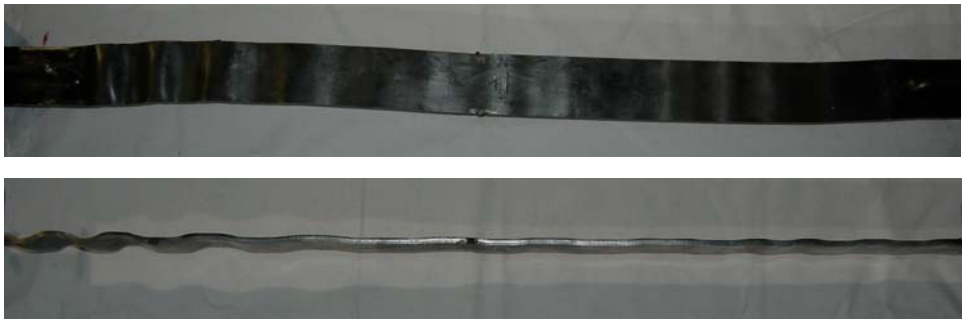

SPECIMEN 12

Figure 2.31 (continued) – Buckling Patterns of Specimens

CHAPTER 3

NUMERICAL STUDY ON BUCKLING RESTRAINED BRACES

3.1 Objectives

The primary objective of the numerical study is to investigate the friction problem that is present for buckling restrained braces. Under compressive forces the core segment expands in both transverse directions due to the Poisson effect as explained in Chapter 1. The core segment should freely expand to minimize the increase in load level under compressive forces. If the expansion is prevented by the encasing member then this restraint causes the core brace to attain higher load levels than expected. The difference between the axial load levels for tension and compression can be significant for V-type concentric braces. In this type of a lateral load resisting system an unbalanced force is created on the beam due to the differences in tensile and compressive brace behavior.

A debonding material is placed between the core brace and the encasing member. The function of the debonding agent is twofold; to reduce the amount of friction at the interface, and to allow the core segment to expand freely. The design and detailing of the debonding layer presents a variety of challenges. Particularly, the thickness and the elastic modulus of the debonding material have to be selected correctly. If the modulus of the debonding agent is too high and the thickness is too small then the core segment may not expand freely. On the other hand, if the modulus is low and the thickness is large then the core segment is prone to local buckling.

Another issue that needs to be considered is the amount of friction transfer. The amount of friction that is transferred to the core segment is directly related to the coefficient of friction (μ) and the amount of contact pressure between the surfaces. The detailing of the debonding agent is also dependent on the geometrical properties of the core and encasing as well as the expected value of the coefficient of friction.

There are no numerical studies reported to date on the behavior of buckling restrained braces with different debonding material configurations. A numerical study

has been undertaken to evaluate various cases of debonding. The following sections present the details of the numerical study conducted to tackle the debonding problem.

3.2 Finite Element Parametric Study on the Debonding Problem

The debonding problem has been studied in a two-dimensional setting in order to reduce the computational costs. Core segment, debonding material, and encasing has been modeled as shown in Fig. 3.1. Basically, the debonding material was assumed to be fully bonded to the core segment. A contact surface has been specified between the debonding material and the encasing member.

A commercially available finite element program ANSYS (2006) was used to conduct the analysis. Two dimensional, 8-node, plane82 elements were used to model the geometry. Mapped meshing was utilized and element sizes were kept below 2 mm. Contact between surfaces has been modeled using a contact pair that utilizes contact172 and target169 elements. Encasing member surface was selected as the target surface and debonding surface has been selected as the contact surface. It was assumed that no initial gap exists between the contacting surfaces.

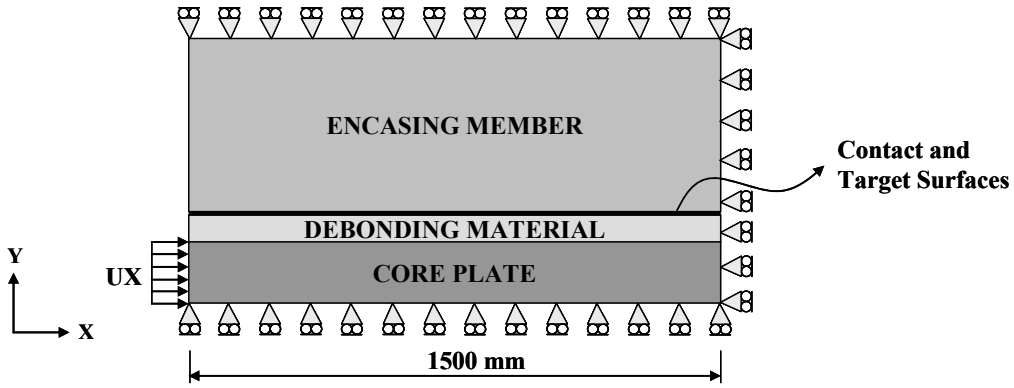

Figure 3.1 – Analytical Model

In all models, displacement was applied at the free end of the core segment such that the overall axial strain of the core reaches 2 percent. The specified boundary conditions are given in Fig. 3.1. A typical finite element mesh is given in Fig. 3.2. In all models the core segment was modeled as steel with bilinear stress-strain behavior. The yield strength and the hardening modulus were taken as 300 MPa and 1 GPa,

respectively. The debonding material and the encasing member were assumed to remain elastic during the entire loading history.

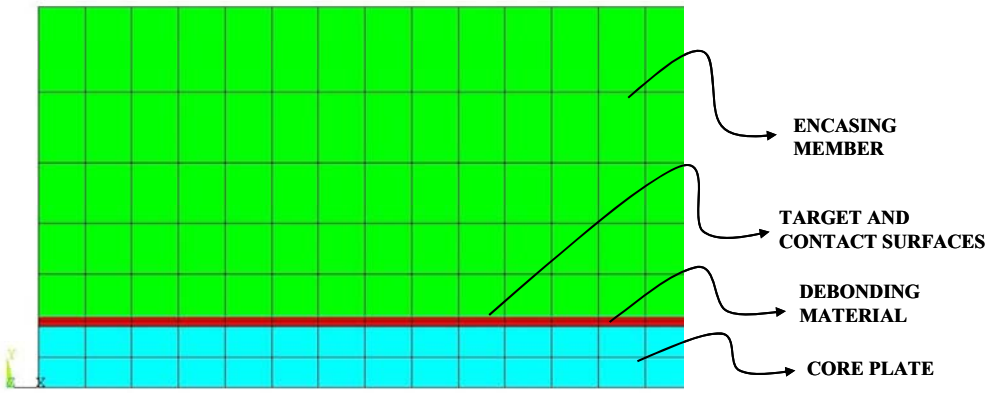

Figure 3.2 – Typical Finite Element Mesh

In general, two sets of parametric studies were conducted to investigate the debonding problem. It is expected that the properties of the encasing member has influence on the analysis results. Basically, when the core segment expands in the transverse direction it comes into contact with the encasing member. The amount of contact pressure that develops is influenced by the material and geometric properties of the encasing member particularly with the elastic modulus and the thickness. For this reason two different sets of analysis which comprise different encasing properties were conducted. In the first set of runs, it was assumed that the encasing member is made up of concrete with a thickness of 50 mm and an elastic modulus of 20 GPa. In the second case, a steel encasing member with 10 mm thickness and 200 GPa elastic modulus was modeled.

For both sets of analyses, thickness and elastic modulus of the debonding material, thickness of core brace, and the friction coefficient (μ) was changed. Core segment thickness values of 5 mm, 10 mm, 15 mm, and 20 mm were considered. The debonding material thickness values were taken as 0.2 mm, 0.5 mm, 1 mm, and 1.5 mm. Elastic modulus values of 0.002 GPa, 0.02 GPa, 0.2 GPa, 2 GPa, 20 GPa and 200 GPa were considered. Finally, analyses were conducted for friction coefficient values of 0, 0.1, 0.25, 0.5, and 1.0.

In all analysis the axial load and displacement at the free end of the core segment were monitored. In addition, plastic strain values along the core segment, and contact/frictional stresses were obtained along the contact surface. A total of 960 nonlinear finite element analyses were conducted. Results are presented for the axial load levels, plastic strains, and frictional stresses in the following sections.

3.3 Axial Load Level

As mentioned before the axial load level attained is influenced by the debonding material properties. In all finite element analyses the axial load level that corresponds to 2 percent strain was recorded. In order to present the results in an effective way axial load values were normalized. Separate sets of analyses were conducted to find out the axial load level for the case where there is no encasing. This case represents a base value. Later axial load level obtained for a particular geometry was normalized with this base value. Results are presented in Tables 3.1 and 3.2 for concrete encased and steel encased core segments, respectively. In these tables, cases with not-converged solutions are given as empty cells and also cases with a maximum of 30 percent and 50 percent increase in axial load levels are shown in grey and dark grey, respectively.

Table 3.1 – Normalized Axial Loads for Concrete Encased Cases

		μ = 0															
Core (mm)		20	15	10	5	20	15	10	5	20	15	10	5	20	15	10	5
Debond (mm)		1.5	1.5	1.5	1.5	1	1	1	1	0.5	0.5	0.5	0.5	0.2	0.2	0.2	0.2
E (Gpa)	200	1.05	1.04	1.03	1.02	1.05	1.04	1.03	1.02	1.05	1.04	1.03	1.02	1.05	1.04	1.03	1.02
	20	1.05	1.04	1.03	1.02	1.05	1.04	1.03	1.02	1.05	1.04	1.03	1.01	1.05	1.04	1.03	1.01
	2	1.05	1.04	1.03	1.02	1.05	1.04	1.03	1.02	1.05	1.04	1.03	1.02	1.05	1.04	1.03	1.01
	0.2	1.02	1.01	1.01	1.01	1.02	1.02	1.01	1.01	1.03	1.02	1.02	1.01	1.04	1.03	1.02	1.01
	0.02	1.00	1.00	1.00	1.00	1.00	1.00	1.00	1.00	1.01	1.00	1.00	1.00	1.01	1.01	1.01	1.00
	0.002	1.00	1.00	1.00	1.00	1.00	1.00	1.00	1.00	1.00	1.00	1.00	1.00	1.00	1.00	1.00	1.00

		μ = 0.1															
Core (mm)		20	15	10	5	20	15	10	5	20	15	10	5	20	15	10	5
Debond (mm)		1.5	1.5	1.5	1.5	1	1	1	1	0.5	0.5	0.5	0.5	0.2	0.2	0.2	0.2
E (Gpa)	200	1.92	1.99	2.08	2.19	1.93	2.01	2.10	2.23	1.95	2.03	2.13	2.27	1.96	2.04	2.15	2.30
	20	2.06	2.14	2.20	2.20	2.06	2.15	2.24	2.29	2.04	2.14	2.26	2.38	2.01	2.10	2.23	
	2	1.95	2.04	2.18	2.46	1.96	2.05	2.18	2.43	1.96	2.05	2.18	2.39	1.96	2.05	2.17	2.35
	0.2	1.42	1.44	1.48	1.56	1.52	1.55	1.59	1.67	1.69	1.73	1.78	1.88	1.83	1.89	1.96	2.08
	0.02	1.04	1.04	1.05	1.05	1.06	1.06	1.07	1.07	1.13	1.13	1.14	1.15	1.30	1.31	1.31	1.33
	0.002	1.00	1.00	1.00	1.01	1.01	1.01	1.01	1.01	1.01	1.01	1.01	1.01	1.03	1.03	1.03	1.03

		μ = 0.25															
Core (mm)		20	15	10	5	20	15	10	5	20	15	10	5	20	15	10	5
Debond (mm)		1.5	1.5	1.5	1.5	1	1	1	1	0.5	0.5	0.5	0.5	0.2	0.2	0.2	0.2
E (Gpa)	200	2.60	2.78	3.02	3.36	2.64	2.83	3.09	3.47	2.68	2.88	3.16	3.58	2.70	2.91	3.20	3.65
	20	2.96	3.22	3.55	3.94	2.94	3.22			2.88	3.15	3.54		2.80			
	2	2.73	2.97	3.36	4.14	2.73	2.97	3.33	4.05	2.72	2.95	3.30	3.91	2.72	2.94	3.26	3.80
	0.2	1.95	2.02	2.13	2.37	2.11	2.21	2.34	2.59	2.36	2.49	2.67	2.97	2.55	2.72	2.96	3.32
	0.02	1.12	1.13	1.14	1.16	1.19	1.20	1.20	1.23	1.37	1.38	1.40	1.43	1.74	1.77	1.80	1.84
	0.002	1.01	1.01	1.01	1.01	1.01	1.01	1.01	1.02	1.03	1.03	1.03	1.03	1.07	1.07	1.07	1.08

Table 3.1 (continued) – Normalized Axial Loads for Concrete Encased Cases

		μ = 0.5															
Core (mm)		20	15	10	5	20	15	10	5	20	15	10	5	20	15	10	5
Debond (mm)		1.5	1.5	1.5	1.5	1	1	1	1	0.5	0.5	0.5	0.5	0.2	0.2	0.2	0.2
E (Gpa)	200	3.31	3.65	4.12	4.83	3.38	3.73	4.26	5.05	3.44	3.83	4.39	5.26	3.48	3.89	4.45	5.36
	20	3.79	4.26	4.95	5.98	3.79	4.29	5.04									
	2	3.56	4.02	4.77	6.29	3.55	4.00	4.72	6.14	3.54	3.97	4.64	5.89	3.52	3.94	4.57	5.61
	0.2	2.59	2.76	3.01	3.52	2.80	3.01	3.32	3.87	3.12	3.41	3.81	4.48	3.24	3.57	3.97	4.79
	0.02	1.28	1.29	1.31	1.37	1.41	1.42	1.45	1.50	1.73	1.76	1.80	1.88	2.30	2.40	2.51	2.65
	0.002	1.02	1.02	1.02	1.03	1.03	1.03	1.03	1.04	1.06	1.06	1.06	1.07	1.18	1.18	1.18	1.18

		μ = 1															
Core (mm)		20	15	10	5	20	15	10	5	20	15	10	5	20	15	10	5
Debond (mm)		1.5	1.5	1.5	1.5	1	1	1	1	0.5	0.5	0.5	0.5	0.2	0.2	0.2	0.2
E (Gpa)	200	4.13	4.72	5.63	7.07	4.23	4.88	5.82	7.62	4.33	5.00	6.12	8.13	4.38	5.12	6.31	8.58
	20	4.62	5.37	6.51	8.48	4.69	5.48	6.75	9.03	4.65	5.46	6.77	9.27	4.55	5.33	6.59	9.03
	2	4.51	5.31	6.70	9.66	4.49	5.28	6.64	9.48	4.46	5.23	6.50	9.11	4.44	5.19	6.44	8.92
	0.2	3.47	3.84	4.40	5.49	3.74	4.19	4.87	6.10	3.83	4.53	5.33	6.15	4.27	4.94	5.60	7.64
	0.02	1.58	1.60	1.65	1.77	1.79	1.83	1.89	2.02	2.31	2.40	2.51	2.70	3.12		3.61	3.75
	0.002	1.04	1.04	1.05	1.06	1.06	1.07	1.07	1.08	1.15	1.15	1.15	1.16	1.40	1.40	1.40	1.41

Table 3.2 – Normalized Axial Loads for Steel Encased Cases

		μ = 0															
Core (mm)		20	15	10	5	20	15	10	5	20	15	10	5	20	15	10	5
Debond (mm)		1.5	1.5	1.5	1.5	1	1	1	1	0.5	0.5	0.5	0.5	0.2	0.2	0.2	0.2
E (Gpa)	200	1.16	1.16	1.16	1.16	1.16	1.16	1.16	1.16	1.16	1.16	1.16	1.16	1.16	1.16	1.16	1.16
	20	1.16	1.16	1.15	1.14	1.16	1.16	1.16	1.14	1.16	1.16	1.16	1.15	1.16	1.16	1.16	1.16
	2	1.13	1.12	1.10	1.07	1.14	1.13	1.11	1.08	1.16	1.15	1.14	1.11	1.16	1.16	1.16	1.16
	0.2	1.02	1.02	1.01	1.01	1.03	1.03	1.02	1.01	1.05	1.04	1.03	1.02	1.10	1.08	1.06	1.06
	0.02	1.00	1.00	1.00	1.00	1.00	1.00	1.00	1.00	1.01	1.01	1.00	1.00	1.02	1.01	1.01	1.01
	0.002	1.00	1.00	1.00	1.00	1.00	1.00	1.00	1.00	1.00	1.00	1.00	1.00	1.00	1.00	1.00	1.00

		μ = 0.1															
Core (mm)		20	15	10	5	20	15	10	5	20	15	10	5	20	15	10	5
Debond (mm)		1.5	1.5	1.5	1.5	1	1	1	1	0.5	0.5	0.5	0.5	0.2	0.2	0.2	0.2
E (Gpa)	200	2.43	2.65	3.02	3.73	2.47	2.72	3.14	4.00	2.52	2.79	3.27	4.34	2.55	2.84	3.36	4.57
	20	2.93	3.36	4.13	5.90	2.87	3.29	4.07	5.97	2.76	3.15	3.90	5.82	2.66	3.01	3.68	5.44
	2	2.53	2.84	3.38	4.70	2.55	2.85	3.41	4.83	2.56	2.87	3.43	4.87	2.56	2.87	3.43	4.82
	0.2	1.54	1.57	1.62	1.74	1.72	1.77	1.84	1.99	2.06	2.17	2.32	2.59	2.34	2.54	2.88	3.53
	0.02	1.04	1.04	1.05	1.05	1.07	1.07	1.07	1.08	1.14	1.14	1.15	1.16	1.38	1.38	1.39	1.41
	0.002	1.00	1.00	1.00	1.01	1.01	1.01	1.01	1.01	1.01	1.01	1.01	1.01	1.03	1.03	1.03	1.03

		μ = 0.25															
Core (mm)		20	15	10	5	20	15	10	5	20	15	10	5	20	15	10	5
Debond (mm)		1.5	1.5	1.5	1.5	1	1	1	1	0.5	0.5	0.5	0.5	0.2	0.2	0.2	0.2
E (Gpa)	200	3.36	3.78	4.47	5.78	3.44	3.91	4.71	6.24	3.53	4.05	4.96	6.94	3.58	4.22	5.11	7.53
	20	4.11	4.85	6.17	9.22	4.04	4.79	6.15	9.50	3.90	4.61	5.93	9.38	3.76	4.41	5.63	8.80
	2	3.62	4.21	5.29	8.01	3.62	4.21	5.30	8.12	3.62	4.21	5.29	7.98	3.62	4.20	5.26	7.94
	0.2	2.22	2.32	2.48	2.82	2.52	2.67	2.90	3.34	2.98	3.27	3.71	4.51	3.34	3.77	4.49	5.97
	0.02	1.13	1.13	1.14	1.16	1.19	1.20	1.21	1.24	1.41	1.41	1.43	1.46	1.90	1.96	2.00	2.06
	0.002	1.01	1.01	1.01	1.01	1.01	1.01	1.01	1.02	1.03	1.03	1.03	1.03	1.08	1.08	1.08	1.08

Table 3.2 (continued) – Normalized Axial Loads for Steel Encased Cases

		μ = 0.5															
Core (mm)		20	15	10	5	20	15	10	5	20	15	10	5	20	15	10	5
Debond (mm)		1.5	1.5	1.5	1.5	1	1	1	1	0.5	0.5	0.5	0.5	0.2	0.2	0.2	0.2
E (Gpa)	200	4.38	5.05	6.14	8.30	4.52	5.28	6.58	9.35	4.66	5.50	7.03	10.92	4.74	5.65	7.34	12.06
	20	5.34	6.42	8.35	12.87	5.30	6.42	8.47	13.55	5.15	6.23	8.27	13.59	4.98	6.00	7.89	12.80
	2	4.81	5.75	7.51	11.98	4.80	5.75	7.53	12.20	4.81	5.75	7.52	12.53	4.80	5.75	7.55	12.73
	0.2	3.10	3.33	3.69	4.43	3.49	3.82	4.33	5.30	4.07	4.62	5.51	7.06	4.47	5.23	6.17	9.48
	0.02	1.29	1.30	1.32	1.37	1.43	1.44	1.46	1.52	1.81	1.84	1.88	1.95	2.68	2.79	2.93	3.12
	0.002	1.02	1.02	1.02	1.03	1.03	1.03	1.03	1.04	1.06	1.06	1.06	1.07	1.18	1.18	1.18	1.19

		μ = 1															
Core (mm)		20	15	10	5	20	15	10	5	20	15	10	5	20	15	10	5
Debond (mm)		1.5	1.5	1.5	1.5	1	1	1	1	0.5	0.5	0.5	0.5	0.2	0.2	0.2	0.2
E (Gpa)	200	5.51	6.52	8.20	11.37	5.73	6.87	8.92	13.41	5.95	7.28	9.74	16.00	6.10	7.52	10.29	17.91
	20	6.72	8.20	10.86	17.14	6.74	8.32	11.26	18.70	6.60	8.18	11.18	19.15	6.41	7.97	10.98	19.64
	2	6.15	7.60	10.33	17.52	6.16	7.64	10.42	18.15	6.19	7.67	10.57	18.90	6.19	7.69	10.60	19.10
	0.2	4.32	4.83	5.60	7.14	4.80	5.50	6.56	8.67	5.36	6.37	8.09	11.68	5.78	6.98	9.36	15.16
	0.02	1.60	1.62	1.66	1.78	1.85	1.88	1.94	2.06	2.54	2.62	2.72	2.90	3.81	4.12	4.51	5.07
	0.002	1.04	1.04	1.05	1.05	1.06	1.07	1.07	1.08	1.14	1.15	1.15	1.16	1.40	1.41	1.41	1.42

Plots of normalized axial loads for different friction coefficients are given in Figs. 3.3 and 3.4. In these figures, legend subscript "C" represents the core plate thickness and "T" represents the debonding layer thickness for the case studied. In general, there is an increase in the normalized axial loads with an increase in the friction coefficient. The following can be observed from the analysis results:

- For μ=0 all geometric and material properties lead to acceptable solutions. If no friction is present at the interface, the maximum increase in load levels is only 5 percent and 15 percent for concrete and steel encased braces, respectively.
- For μ=0.1 using a debonding material with an elastic modulus of either 0.002 GPa or 0.02 GPa produces acceptable solutions for all of the cases except a few. Particularly, 0.2 mm thick debonding material with a 0.02 GPa modulus leads to load increases on the order of 35 percent. In addition, 1.5 mm thick debonding material with a 0.2 GPa modulus leads to load increases in the range of 30 to 50 percent for concrete encased braces only.
- For μ=0.25 using a debonding material with an elastic modulus of 0.002 GPa produces acceptable solutions for all cases. Furthermore, an elastic modulus value of 0.02 GPa produces acceptable solutions for debonding thickness equal to and larger than 1 mm. For cases with 0.02 GPa elastic modulus and 0.5 mm debonding thickness axial load increases are in the range of 30 to 50 percent.
- For μ=0.5 using a debonding material with an elastic modulus of 0.002 GPa produces acceptable solutions for all cases. In addition, an elastic modulus value of 0.02 GPa leads to axial load increases on the order of 30 to 50 percent for debonding thickness equal to and larger than 1 mm.
- For μ=1 using a debonding material with an elastic modulus of 0.002 GPa seems to be the only viable solution. Other modulus values produce normalized axial load levels in excess of 1.5. Among the cases with 0.002 GPa elastic modulus, debonding thickness of 0.2 mm are problematic. In these cases the normalized axial load levels surpass 1.3.

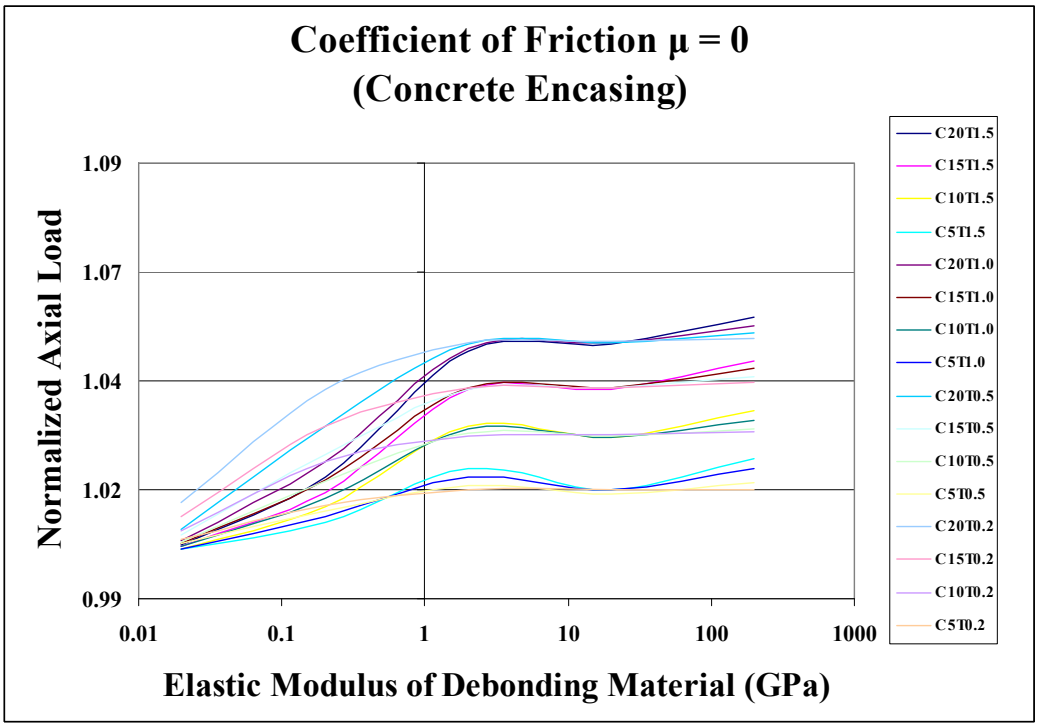

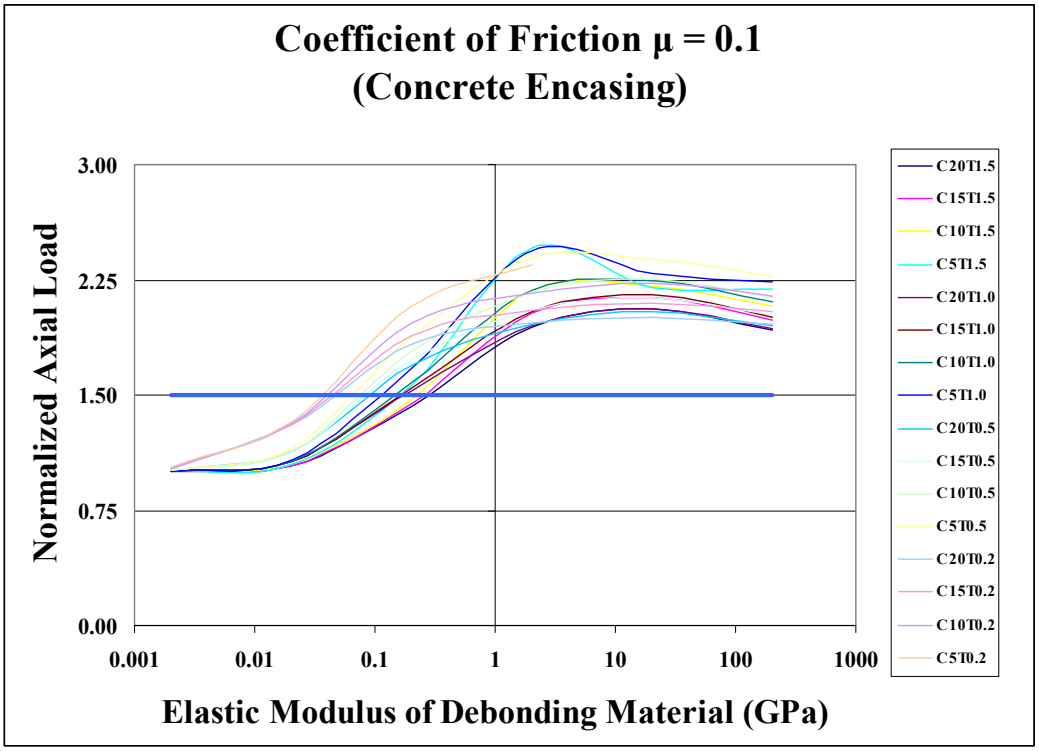

Figure 3.3 – Normalized Axial Loads for Concrete Encased Cases

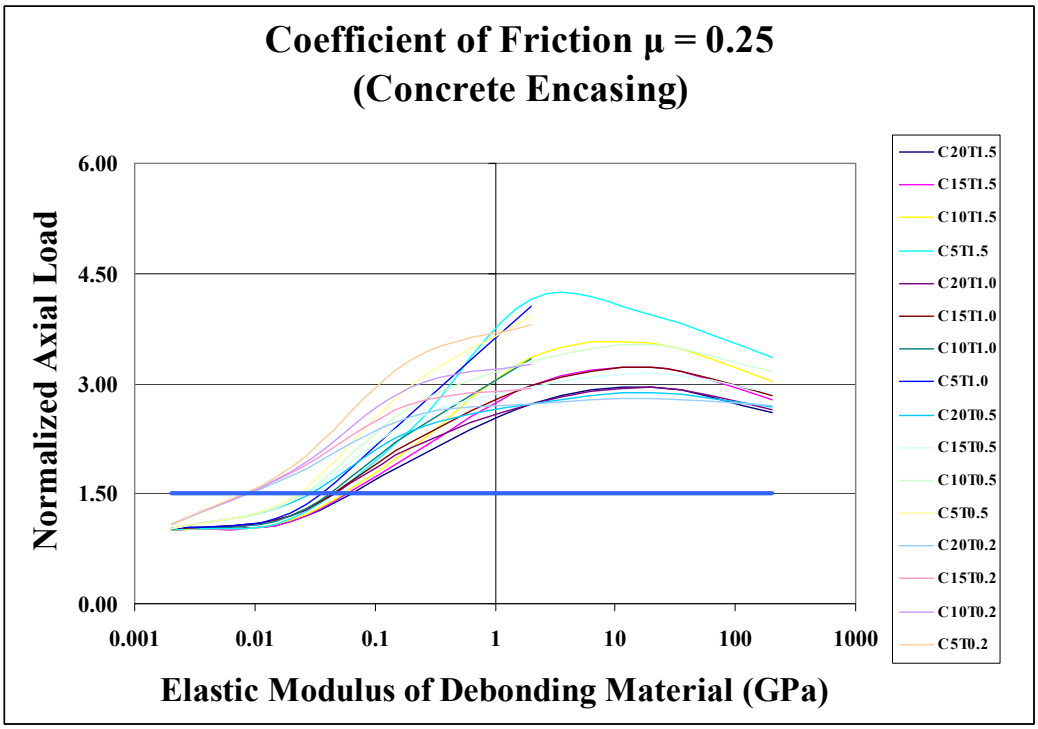

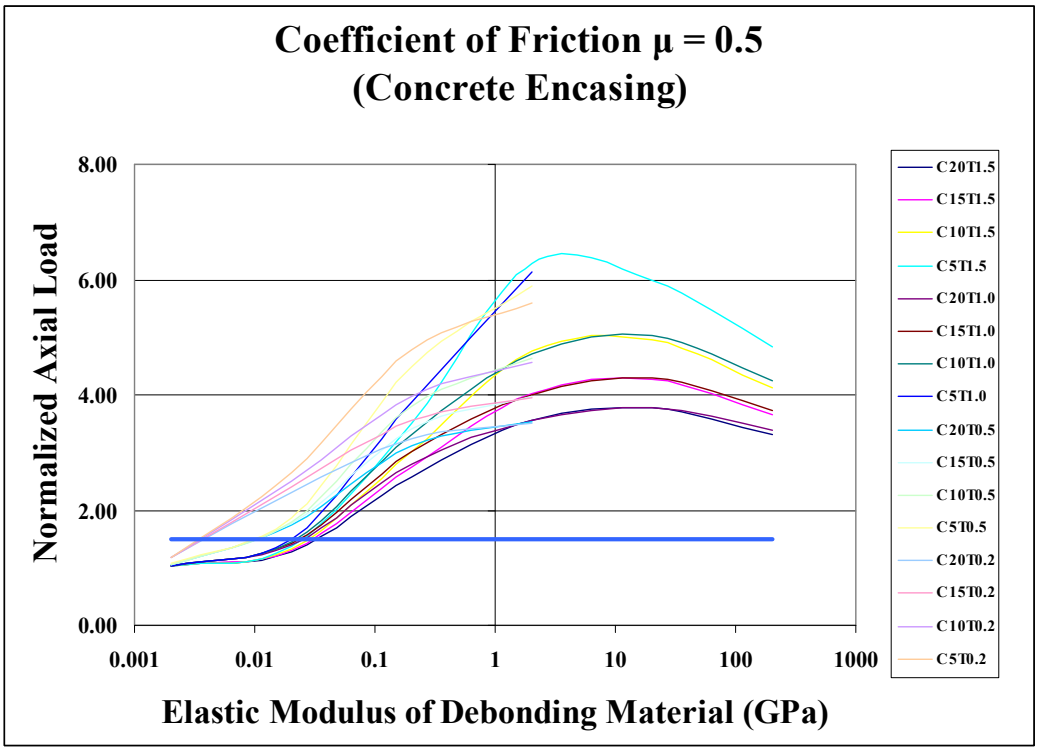

Figure 3.3 (continued) – Normalized Axial Loads for Concrete Encased Cases

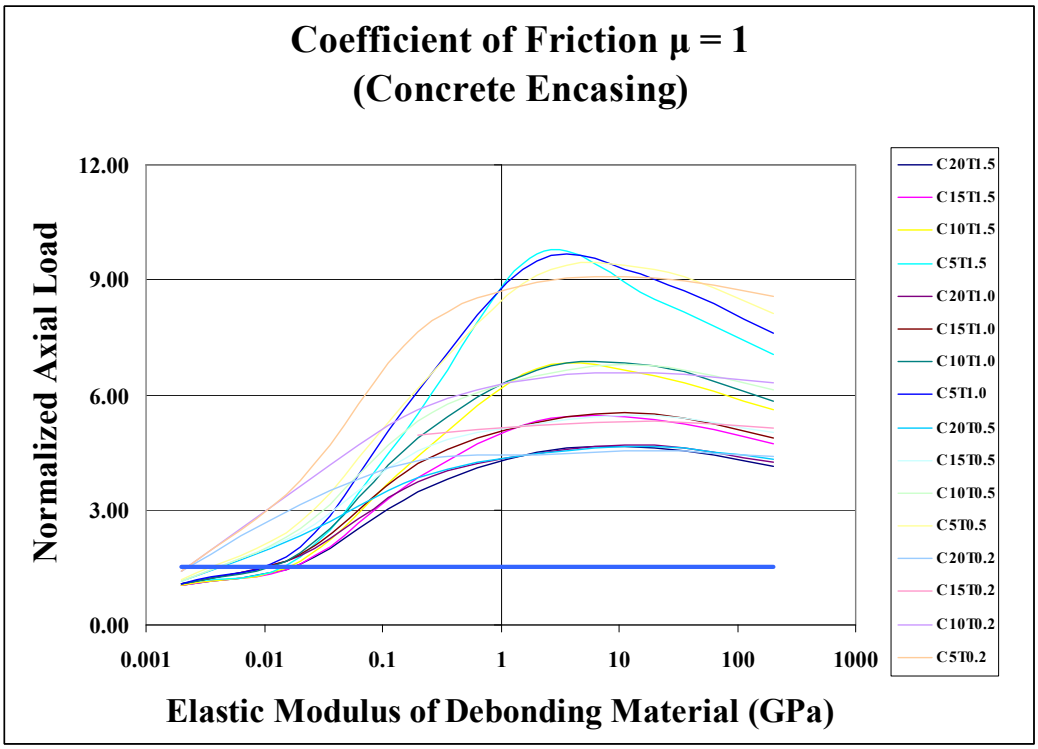

Figure 3.3 (continued) – Normalized Axial Loads for Concrete Encased Cases

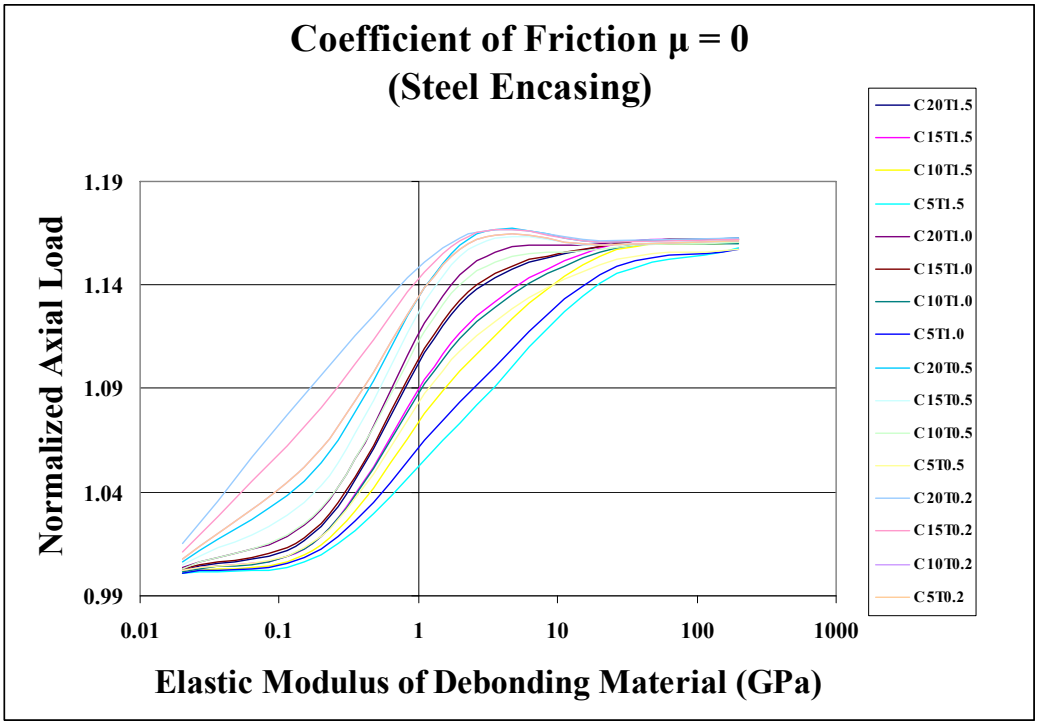

Figure 3.4 – Normalized Axial Loads for Steel Encased Cases

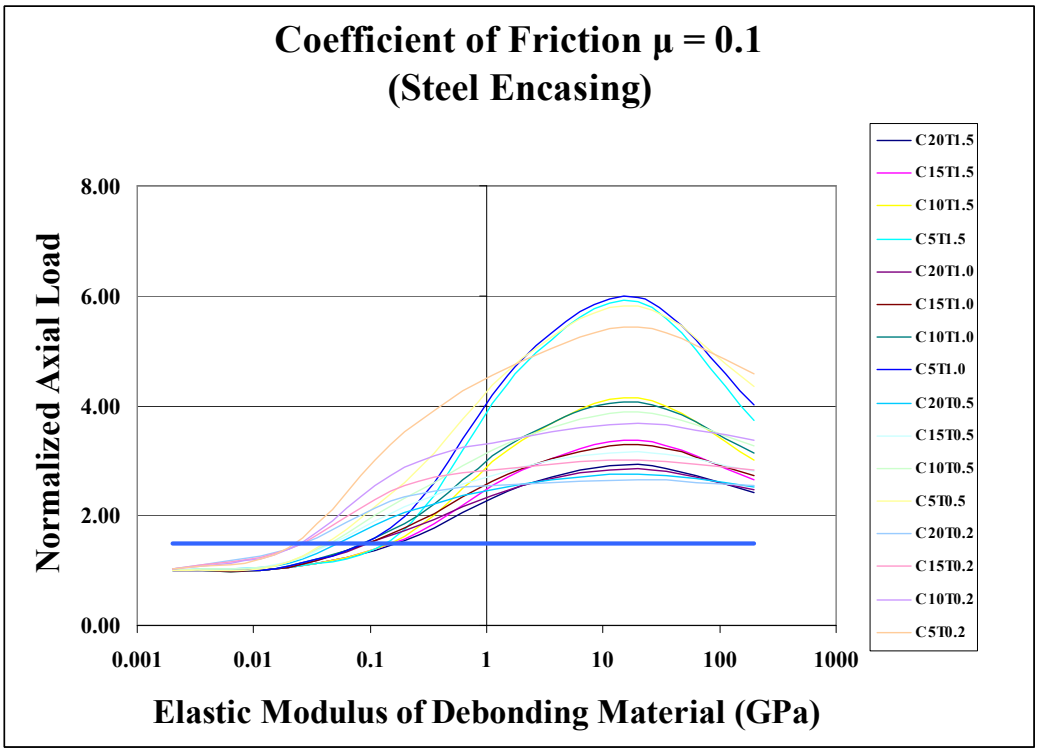

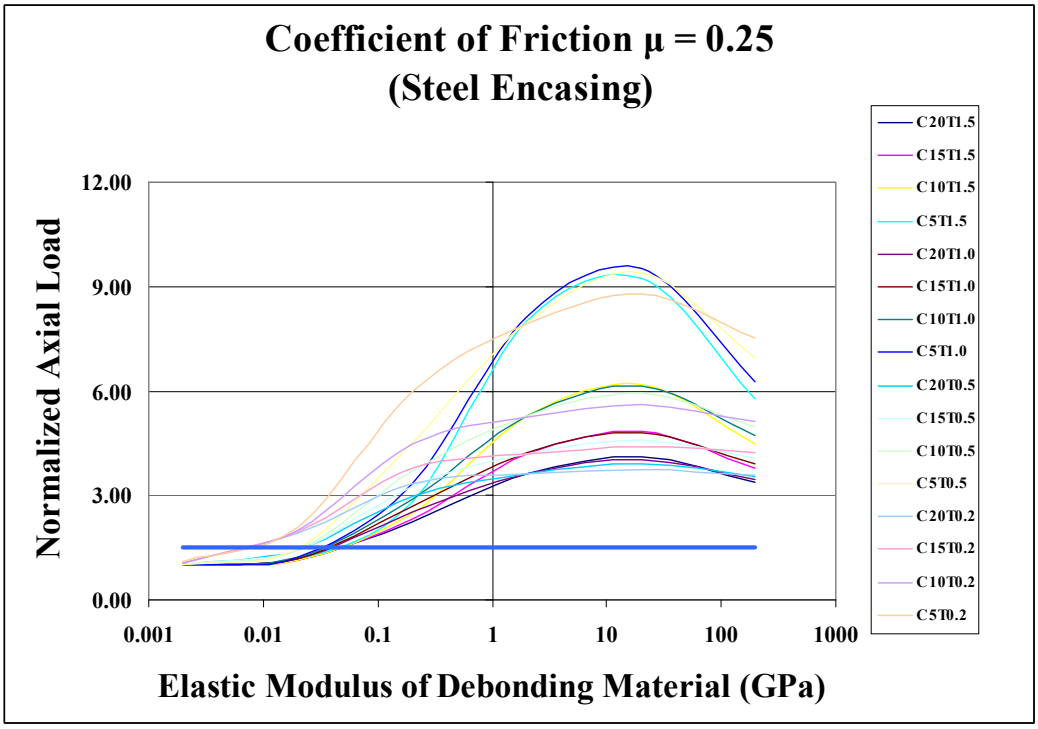

Figure 3.4 (continued) – Normalized Axial Loads for Steel Encased Cases

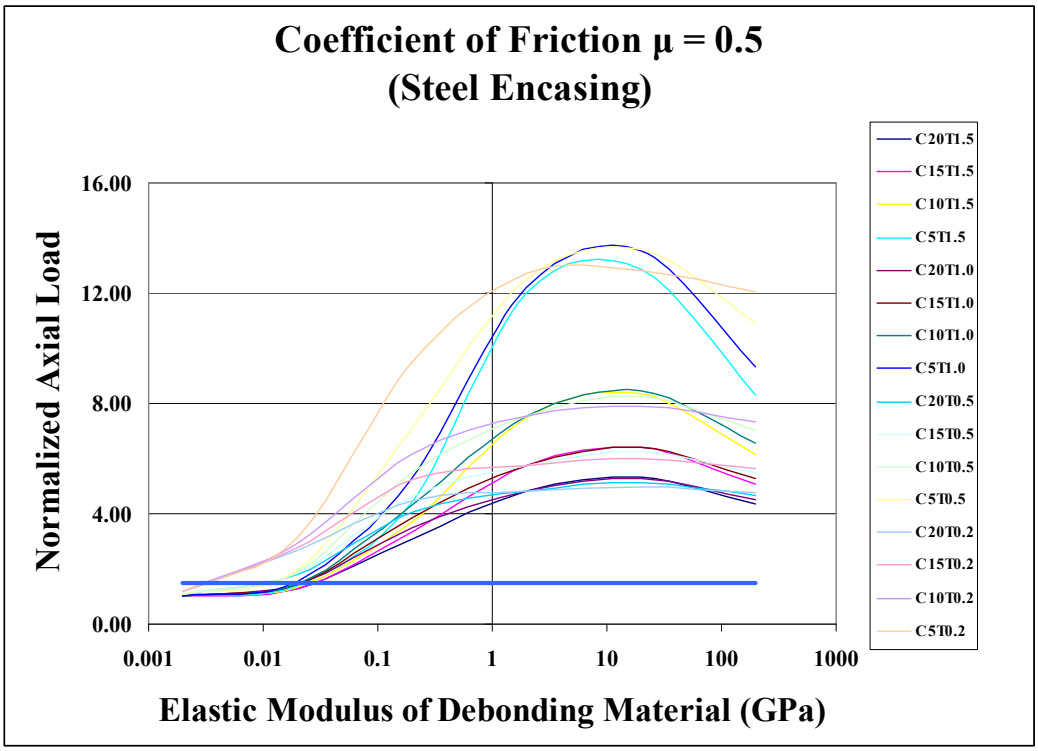

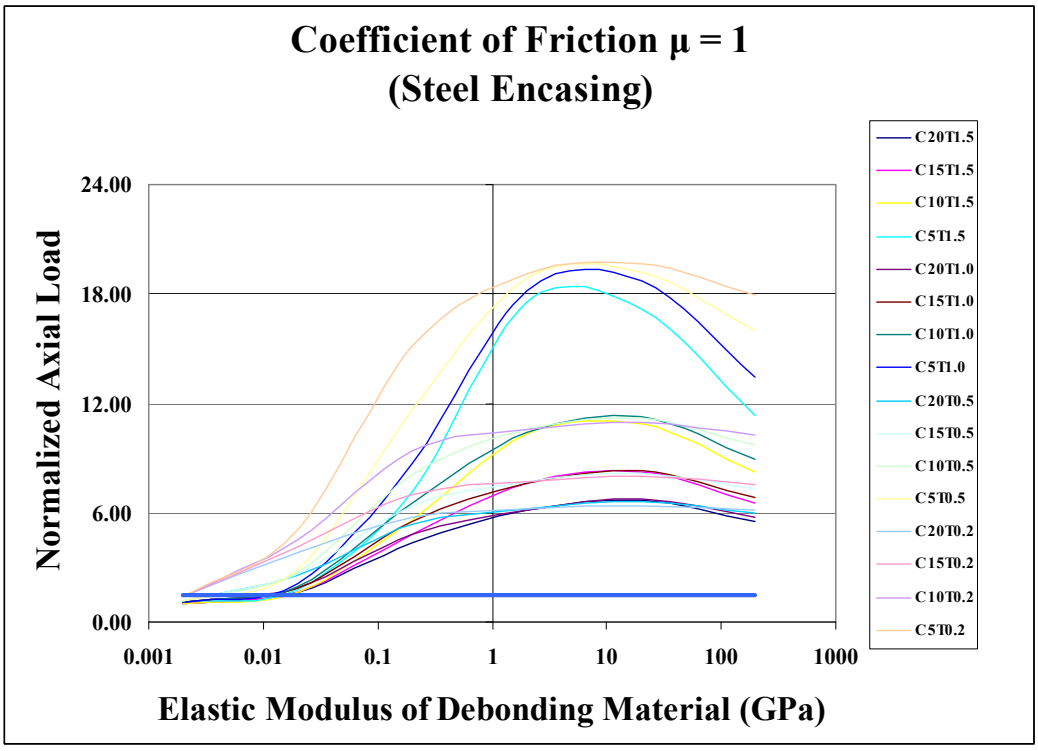

Figure 3.4 (continued) – Normalized Axial Loads for Steel Encased Cases

3.4 Plastic Strains and Frictional Stresses

Another point that is of interest is the variation of plastic strains along the core segment. A satisfactory BRB design should ensure uniform straining of the core segment. If uniform straining cannot be achieved then some portion of the core segment can be subjected to higher strains than expected. Large local strains can cause local buckling at early loading cycles especially in the case of reversed loading. The amount of axial strain at any location along the length of the core is directly related to the variation of frictional stresses along the length.

For all analysis plastic strains and frictional stresses were computed along the length of the member. Results are too numerous to present. However, results for some particular cases are presented herein to show the general trends in behavior.

In the following presentation two cases with debonding modulus values of 0.002 GPa and 2 GPa will be covered. Particularly, a core brace with 5 mm thickness is considered. In Figs. 3.5 and 3.6 variation of plastic strains along the length of the member are given for different debond thicknesses and friction coefficient. It is evident from these figures that uniform straining can be achieved when the friction coefficient is zero. For higher friction coefficients the variation of plastic strains becomes non-uniform. Deviation from a uniform behavior is more pronounced as the friction coefficient increases. Also the non-uniform strain patterns are more pronounced for thinner debonding layers. For cases with a debonding material modulus of 2 GPa only the first few hundreds of millimeters are subjected to high axial strains and the rest of the core segment is virtually strain free for all nonzero friction coefficients.

Representative plots of frictional stresses along the length are given in Fig. 3.7 and 3.8 for the previous cases of interest. As shown in those figures, large frictional stresses form close to the free end of the core brace. These frictional stresses are more pronounced for debonding modulus value of 2 GPa as compared to the ones for 0.002 GPa. In all cases the magnitude of frictional stresses decrease with an increase in the debonding material thickness and a decrease in the friction coefficient.

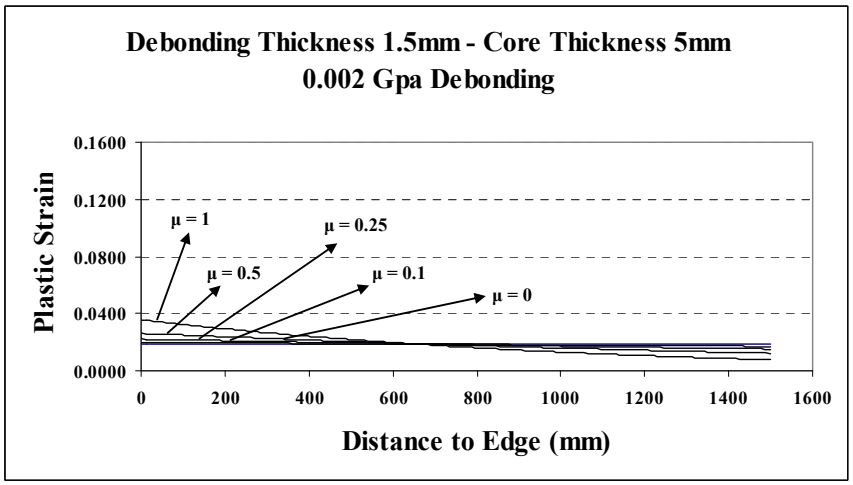

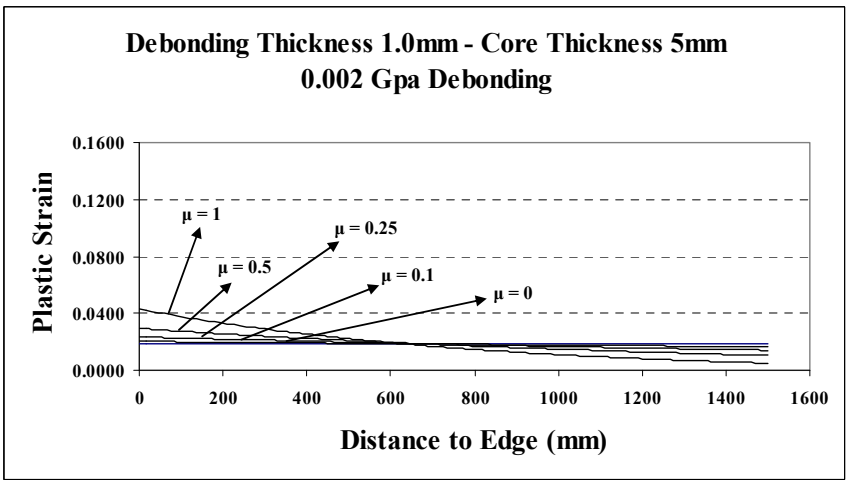

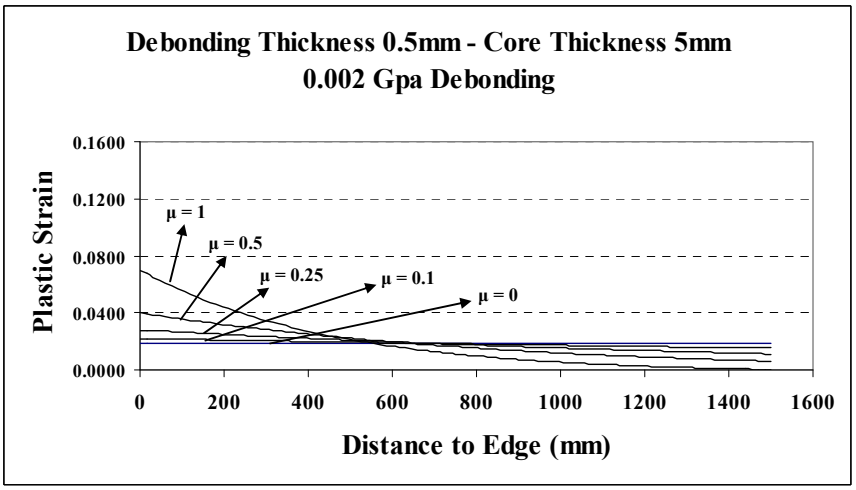

Figure 3.5 – Plastic Strain Variations for 0.002 GPa Debonding

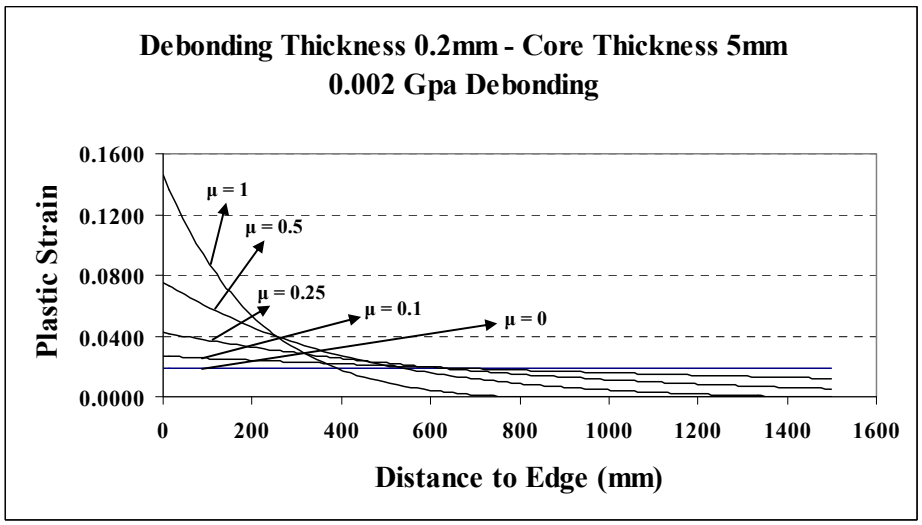

Figure 3.5 (continued) – Plastic Strain Variations for 0.002 GPa Debonding

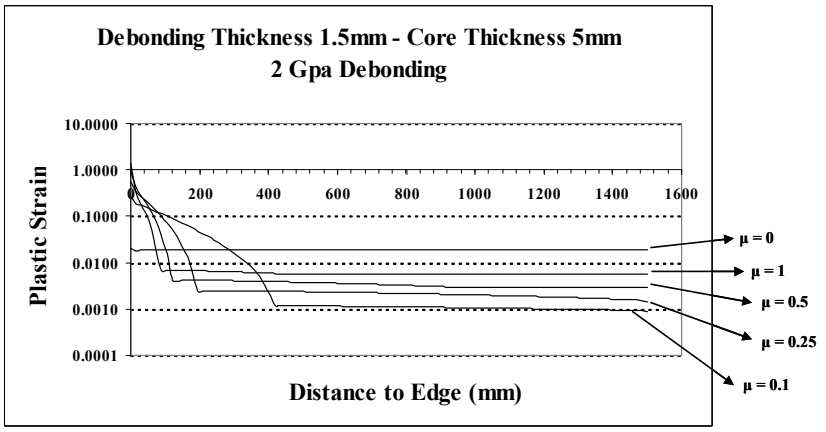

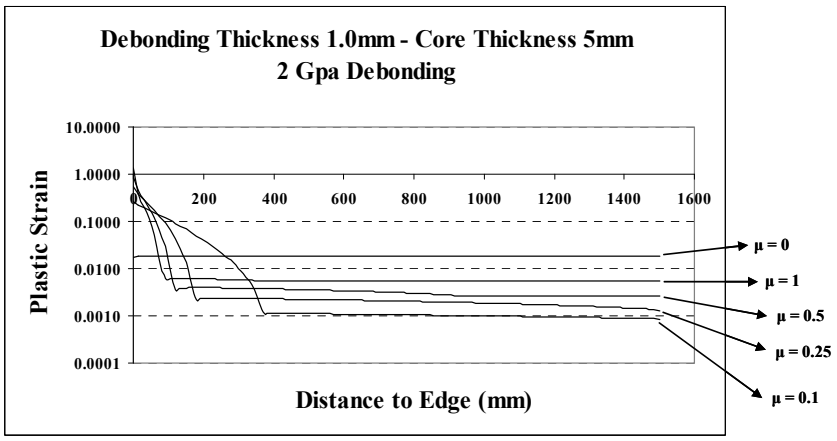

Figure 3.6 – Plastic Strain Variations for 2 GPa Debonding

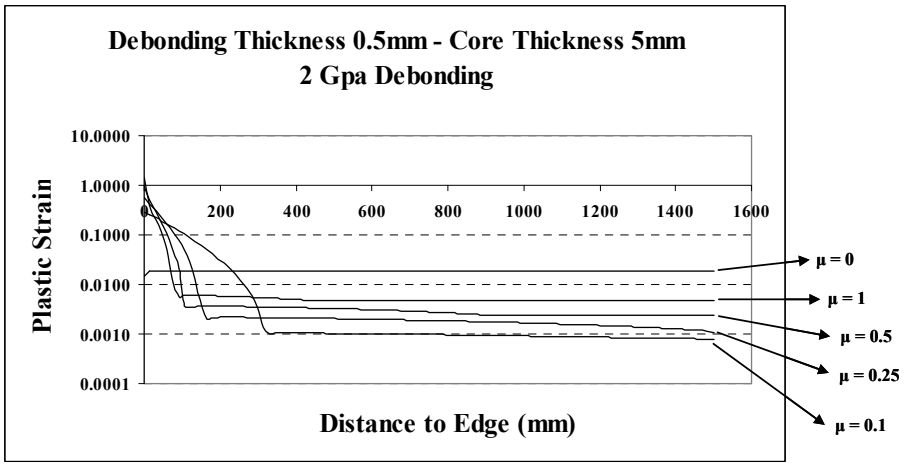

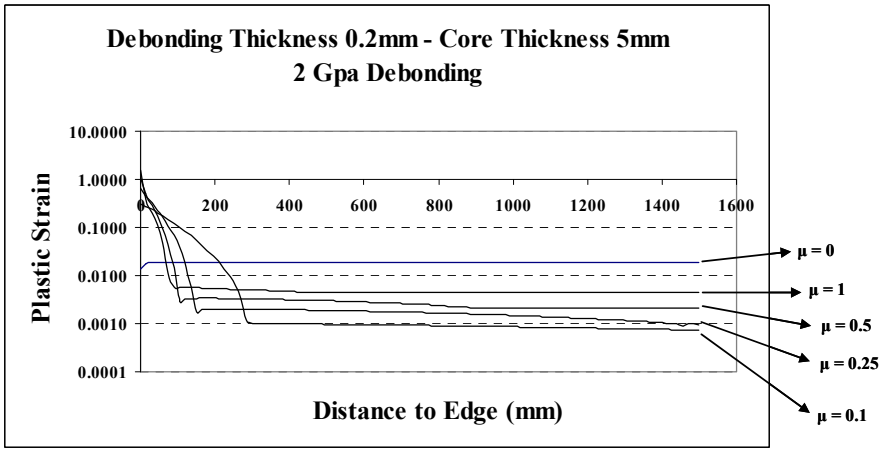

Figure 3.6 (continued) – Plastic Strain Variations for 2 GPa Debonding

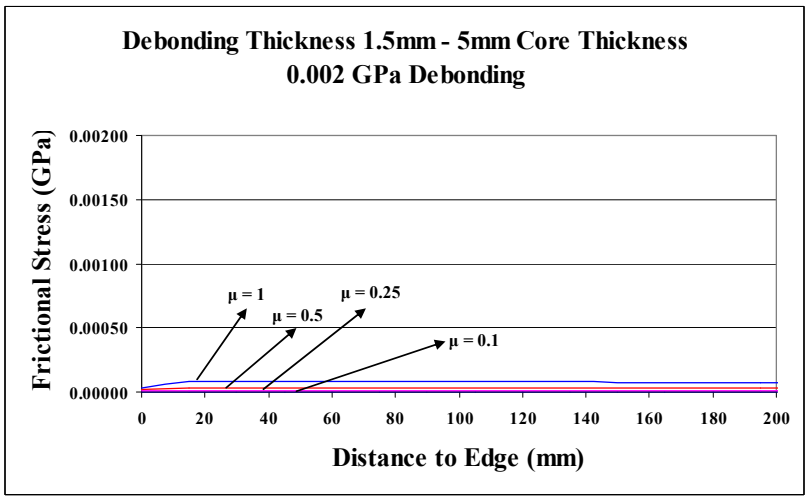

Figure 3.7 – Frictional Stress Variations for 0.002 GPa Debonding

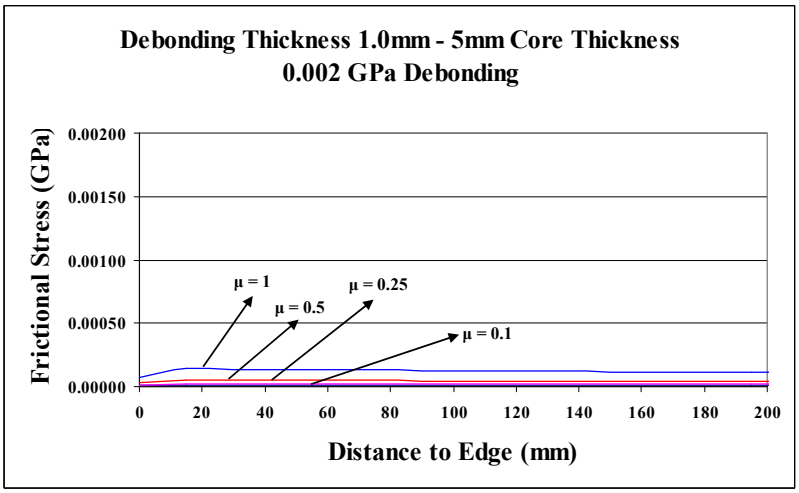

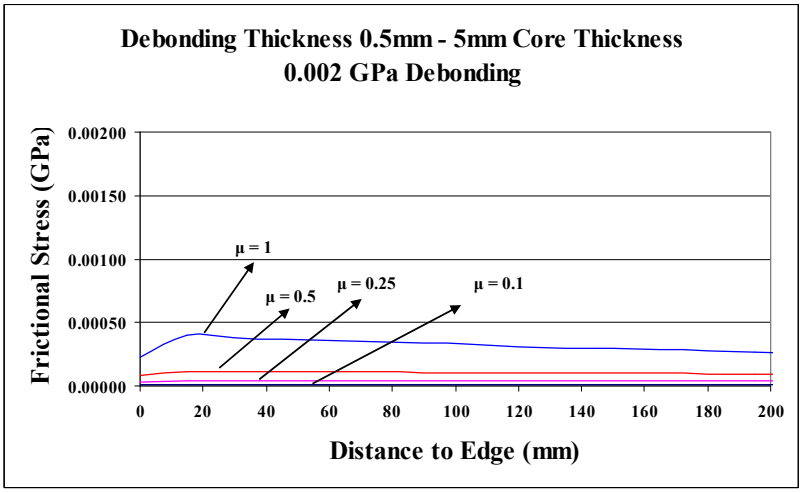

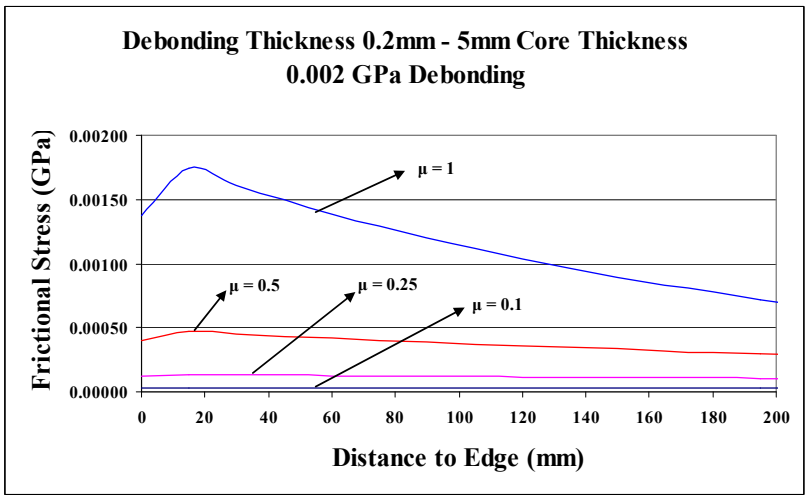

Figure 3.7 (continued) – Frictional Stress Variations for 0.002 GPa Debonding

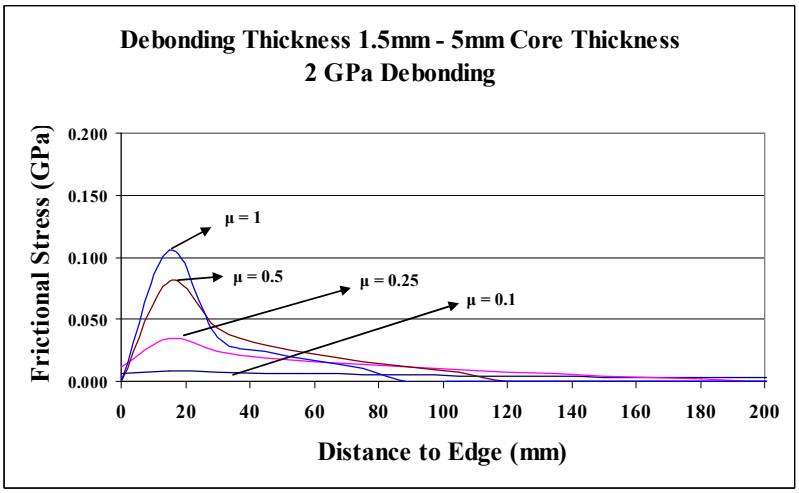

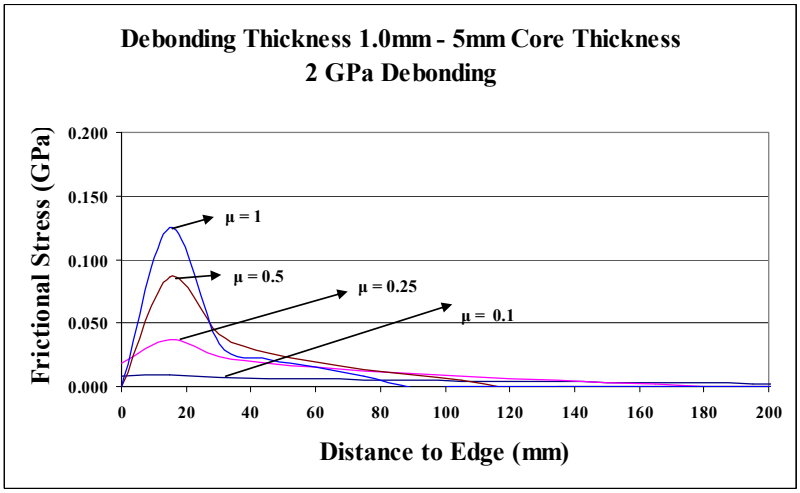

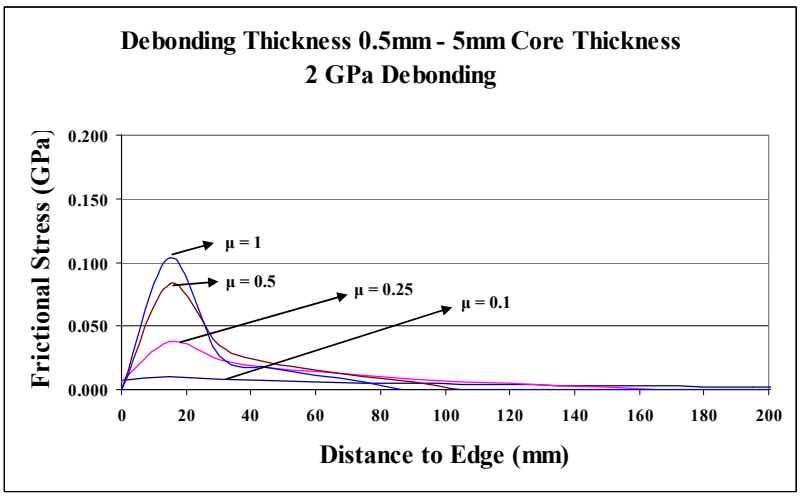

Figure 3.8 – Frictional Stress Variations for 2 GPa Debonding

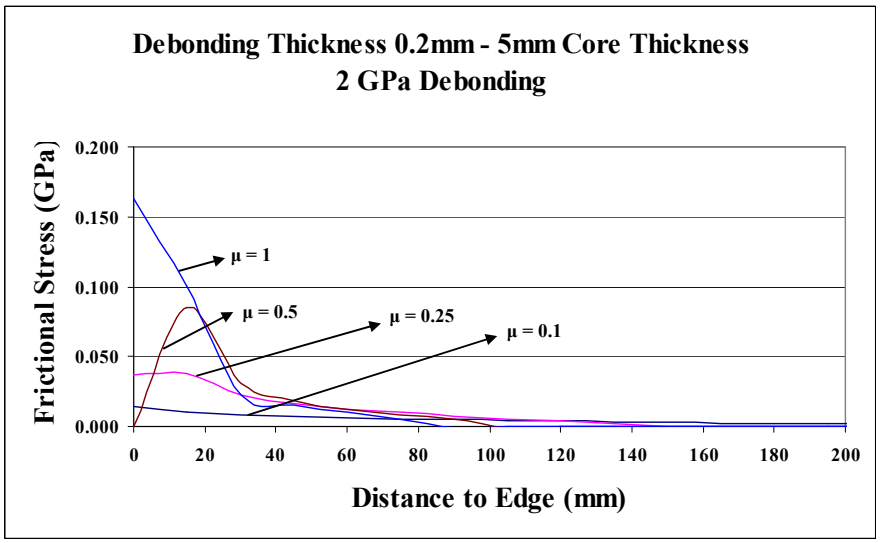

Figure 3.8 (continued) – Frictional Stress Variations for 2 GPa Debonding

Usually the maximum amount of plastic strain that is experienced by the core brace is of interest in the design of a BRB. For this reason, the maximum amount of plastic strain that usually occurs at the very end of the brace is normalized by the overall plastic strain value and the results are given in Tables 3.3 and 3.4. In these tables, only the cases that were found acceptable according to the normalized axial load levels are presented and the cases with a maximum of 100 percent increase in the plastic strain values are shown in grey. It is apparent from this figure that although some geometries can be acceptable according to the amount of axial load increase, they may lead to large local strain demands

Table 3.3 - Normalized Plastic Strain Values for Concrete Encased Cases

		μ = 0															
Core (mm)		20	15	10	5	20	15	10	5	20	15	10	5	20	15	10	5
Debond (mm)		1.5	1.5	1.5	1.5	1	1	1	1	0.5	0.5	0.5	0.5	0.2	0.2	0.2	0.2
E (Gpa)	200	1.01	1.00	1.01	1.00	1.01	1.01	1.00	1.01	1.01	1.01	1.00	1.00	1.01	1.01	1.00	1.00
	20	1.00	1.00	1.00	1.00	1.00	1.00	1.00	1.00	1.00	1.00	1.00	1.00	1.01	1.00	1.00	1.00
	2	1.00	1.00	1.00	1.00	1.00	1.00	1.00	1.00	1.00	1.00	1.00	1.00	1.01	1.00	1.00	1.00
	0.2	1.00	1.00	1.00	1.00	1.00	1.00	1.00	1.00	1.00	1.00	1.00	1.00	1.00	1.00	1.00	1.00
	0.02	1.00	0.99	1.00	1.00	0.99	0.99	1.00	1.00	1.00	1.00	1.00	1.00	1.00	1.00	1.00	1.00
	0.002	1.00	1.00	1.00	1.00	1.00	1.00	1.00	1.00	1.00	1.00	1.00	1.00	0.99	0.99	0.99	0.99
		μ = 0.1															
Core (mm)		20	15	10	5	20	15	10	5	20	15	10	5	20	15	10	5
Debond (mm)		1.5	1.5	1.5	1.5	1	1	1	1	0.5	0.5	0.5	0.5	0.2	0.2	0.2	0.2
E (Gpa)	0.2	6.19	6.66	7.37													
	0.02	1.64	1.67	1.72	1.87	1.95	1.99	2.05	2.22	2.91	3.00	3.13	3.36	5.04	5.30	5.65	6.14
	0.002	1.06	1.06	1.06	1.07	1.08	1.08	1.09	1.10	1.17	1.17	1.17	1.19	1.41	1.41	1.42	1.44
		μ = 0.25															
Core (mm)		20	15	10	5	20	15	10	5	20	15	10	5	20	15	10	5
Debond (mm)		1.5	1.5	1.5	1.5	1	1	1	1	0.5	0.5	0.5	0.5	0.2	0.2	0.2	0.2
E (Gpa)	0.02	2.95	3.04	3.22	3.70	3.96	4.09	4.30	4.82	6.54	6.85	7.25	7.96				
	0.002	1.15	1.15	1.16	1.19	1.22	1.23	1.24	1.27	1.46	1.46	1.48	1.51	2.18	2.20	2.23	2.28
		μ = 0.5															
Core (mm)		20	15	10	5	20	15	10	5	20	15	10	5	20	15	10	5
Debond (mm)		1.5	1.5	1.5	1.5	1	1	1	1	0.5	0.5	0.5	0.5	0.2	0.2	0.2	0.2
E (Gpa)	0.02	5.46	5.70	6.10	7.11	7.30	7.65	8.16									
	0.002	1.32	1.33	1.35	1.41	1.48	1.49	1.51	1.58	2.02	2.04	2.07	2.16	3.85	3.88	3.95	4.08
		μ = 1															
Core (mm)		20	15	10	5	20	15	10	5	20	15	10	5	20	15	10	5
Debond (mm)		1.5	1.5	1.5	1.5	1	1	1	1	0.5	0.5	0.5	0.5	0.2	0.2	0.2	0.2
E (Gpa)	0.002	1.70	1.72	1.77	1.92	2.07	2.10	2.16	2.32	3.42	3.47	3.55	3.76	7.30	7.44	7.58	7.89

Table 3.4 – Normalized Plastic Strain Values for Steel Encased Cases

F																	
μ = 0																	
Core (mm)		20	15	10	5	20	15	10	5	20	15	10	5	20	15	10	5
Debond (mm)		1.5	1.5	1.5	1.5	1	1	1	1	0.5	0.5	0.5	0.5	0.2	0.2	0.2	0.2
E (Gpa)	200	1.10	1.09	1.08	1.05	1.10	1.10	1.08	1.05	1.11	1.10	1.08	1.05	1.11	1.10	1.08	1.05
	20	1.10	1.08	1.07	1.03	1.10	1.09	1.07	1.04	1.11	1.10	1.08	1.05	1.11	1.10	1.08	1.05
	2	1.01	1.00	1.00	1.00	1.01	1.01	1.00	1.00	1.04	1.03	1.01	1.00	1.07	1.06	1.04	1.01
	0.2	1.00	1.00	1.01	1.01	1.00	1.00	1.00	1.01	1.00	1.00	1.00	1.00	1.00	1.00	1.00	0.99
	0.02	1.00	1.00	1.00	1.00	1.00	1.00	1.00	1.00	1.00	1.00	1.00	1.00	1.00	1.00	1.00	1.00
	0.002	1.00	1.00	1.00	1.00	1.00	1.00	1.00	1.00	1.00	1.00	1.00	1.00	1.00	1.00	1.00	1.00
μ = 0.1																	
Core (mm)		20	15	10	5	20	15	10	5	20	15	10	5	20	15	10	5
Debond (mm)		1.5	1.5	1.5	1.5	1	1	1	1	0.5	0.5	0.5	0.5	0.2	0.2	0.2	0.2
E (Gpa)	0.02	1.66	1.69	1.75	1.90	1.99	2.03	2.10	2.27	3.08	3.18	3.32	3.58	5.97	6.32	6.78	7.45
	0.002	1.06	1.06	1.06	1.07	1.08	1.08	1.09	1.10	1.17	1.17	1.18	1.19	1.43	1.43	1.44	1.46
μ = 0.25																	
Core (mm)		20	15	10	5	20	15	10	5	20	15	10	5	20	15	10	5
Debond (mm)		1.5	1.5	1.5	1.5	1	1	1	1	0.5	0.5	0.5	0.5	0.2	0.2	0.2	0.2
E (Gpa)	0.02	2.97	3.07	3.24	3.73	4.01	4.15	4.37	4.91	6.97	7.30	7.72	8.48				
	0.002	1.15	1.15	1.16	1.19	1.22	1.23	1.24	1.27	1.46	1.47	1.48	1.51	2.24	2.26	2.29	2.34
μ = 0.5																	
Core (mm)		20	15	10	5	20	15	10	5	20	15	10	5	20	15	10	5
Debond (mm)		1.5	1.5	1.5	1.5	1	1	1	1	0.5	0.5	0.5	0.5	0.2	0.2	0.2	0.2
E (Gpa)	0.02	5.51	5.75	6.14	7.17	7.53	7.87	8.36									
	0.002	1.32	1.33	1.35	1.41	1.48	1.49	1.51	1.58	2.02	2.04	2.07	2.15	3.89	3.95	4.02	4.16
μ = 1																	
Core (mm)		20	15	10	5	20	15	10	5	20	15	10	5	20	15	10	5
Debond (mm)		1.5	1.5	1.5	1.5	1	1	1	1	0.5	0.5	0.5	0.5	0.2	0.2	0.2	0.2
E (Gpa)	0.002	1.69	1.72	1.77	1.92	2.06	2.09	2.15	2.31	3.37	3.42	3.50	3.70	7.43	7.56	7.72	8.06

Filtering the results of the analyses, which are given below for the axial load level thresholds, with a limit of 100 percent increase in plastic strain demands, following observations can be made:

- For μ=0 all geometric and material properties lead to admissible solutions for both for steel and concrete encasing. In the absence of friction, plastic strain increase reaches 1 percent and 11 percent for concrete and steel encasing, respectively.
- For μ=0.1 using a debonding material with an elastic modulus of 0.002 GPa produces acceptable solutions for both concrete and steel encased braces. In the case of selecting a debonding material with an elastic modulus of 0.02 GPa, 1.5 mm thickness of debonding material with all geometries of core plate and 1.0 mm thickness of debonding material with 20mm and 15mm thicknesses of core plate are admissible for concrete encasing. Same solutions are acceptable also for steel encasing except for the case with core plate and debonding material thicknesses of 15mm and 1mm, respectively.
- For μ=0.25 using a debonding material with an elastic modulus of 0.002 GPa is the only admissible solution for all the cases with 1.5mm, 1.0mm and 0.5mm debonding material thickness in the case of both concrete and steel encasing. Among the cases with 0.002 GPa elastic modulus, debonding material thickness of 0.2 mm leads to an increase in the plastic strain demands beyond 100 percent and are considered as problematic.
- For μ=0.5 using a debonding material with an elastic modulus of 0.002 GPa is the only acceptable solution again. Compared to μ=0.25, acceptability of the results are limited to the cases with debonding material thickness of 1.5 mm and 1.0 mm for both concrete and steel encased braces.
- For μ=1 using a debonding material with an elastic modulus of 0.002 GPa is the only solution for the cases with 1.5 mm debonding material thickness. Both concrete and steel encasing seem acceptable with the given material and geometric properties. Among other geometries of debonding, 0.2 mm thickness gives normalized plastic strain levels in excess of 7.

CHAPTER 4

CONCLUSIONS AND RECOMMENDATIONS FOR FUTURE RESEARCH

4.1 Conclusions

The following can be concluded from experimental study:

- Steel encased BRBs tested as a part of the research program showed satisfactory performance except for one specimen. Steel encasing can be an alternative to mortar filled steel tubes.
- Rolled or built-up shapes can be used for encasing. Built-up sections provide lighter encasings because of the freedom in optimizing its shape.
- Both welded and bolted attachments can be used for connecting the encasing members together. BRBs with welded encasing are lighter when compared with their counterparts.
- Tack welding the core segment to one of the encasing members can be an acceptable solution for preventing the slipping of encasing.
- Continuous welding and snug-tight bolting can create significant amount of frictional resistance at the core-to-encasing interface.
- Imperfections due to manufacturing are not detrimental in terms of the global load deformation response; however, these can lead to early local buckling.
- Steel core segments with an aspect ratio of 16 can show satisfactory performance

Numerical study can be reduced as follows:

- In the absence of friction all geometric and material properties studied produce acceptable solutions from the point of increase in the axial load and plastic strain levels view.
- In the presence of friction number of admissible solutions reduces as a result of the increase in normalized axial load and plastic strain levels.

- In general, some cases below axial load level thresholds are eliminated from the acceptable solutions category after plastic strain demand filtering. As the coefficient of friction increases beyond 0.1, solutions tend to become inadmissible.
- Elastic modulus of 0.002 GPa for debonding material provides acceptable solutions for different combinations of core plate and debonding material geometries in the presence of friction with a coefficient varying from 0.1 to 1.
- For design purposes, μ can be taken as 0.1 and for this case debonding material with an elastic modulus of 0.002 GPa is the only viable solution for all the geometries studied.

4.2 Recommendations for Future Research

Experimental study was limited to small scale component testing. Future research should consider applying the findings of this study to full scale specimens. In addition, spacing of welds and bolts should be studied to minimize the amount of fasteners. Component testing should be extended to sub-assemblage testing to investigate the end connection behavior of steel encased BRBs.

Numerical study was limited to the investigation of the effect of friction between debonding material and encasing member in terms of axial load and plastic strain levels reached. Local buckling of core plates should be studied in future research. Relations between findings of local buckling study and this study should be investigated to come up with a complete solution for design optimization of the ratio between the core plate and the debonding material thicknesses.

REFERENCES

American Institute of Steel Construction (AISC), *Specifications for Structural Steel buildings*, 2005

ANSYS, *Version 6.1 On-line User's Manual*, 2001

Black, C.J., Makris, N., and Aiken, I.D., *Component Testing, Stability Analysis and Characterization of Buckling Restrained Braces*, Rep. No. PEER 2002/08, University of California, Berkeley, California, 2002

BS 3692, *Specification for Iso-metric Precision Hexagon Bolts, Screws and Nuts*, British Standards Institute, London, 2001

Chen, C.C., Chen, S.Y., and Liaw, J.J., *Application of Low Yield Strength Steel on Controlled Plastification Ductile Concentrically Braced Frames*, Canadian Journal of Civil Engineering, 2001a

EN 10025, *Hot Rolled Products of Non-alloy Structural Steel*, European Committee for Standardization, CEN, Brussels, 1994

Fujimoto, M., Wada, A., Saeki, E., Watanabe, A., and Hitomi, Y., *A Study on Unbonded Braces Encased in Buckling-Restraining Concrete and Steel Tube,* Journal of Structural and Construction Engineering, Architectural Institute of Japan, 1988, [in Japanese]

Inoue, K., Sawaizumi, S., Higashibata, Y., and Inoue, K., *Bracing Design Criteria of the Reinforced Concrete Panel Including Unbonded Steel Diagonal Braces*, Journal of Structural and Construction Engineering , Architectural Institute of Japan, 1992 [in Japanese]

Iwata, M., Kato, T., and Wada, A., *Buckling-Restrained Braces as Hysteretic Dampers*, Proceedings, STESSA, Quebec, 2000

Iwata, M., and Murai, M, *Buckling-Restrained Brace Using Steel Mortar Planks; Performance Evaluation as a Hysteretic Damper*, Earthquake Engineering and Structural Dynamics, 2006

Manabe, N., Simokawa, H., Kamiya, M., Morino, S., and Kawaguchi, J., *Elasto-Plastic Behavior of Flat-Bar Brace Stiffened by Square Steel Tube*, AIJ, 1996 [in Japanese]

Murakami, E., Mitarai, Y., Asayama, N., and Narihara, H., *Experiment on Retrofitting of Exiting Brace Improved to Unbonded Brace*, AIJ, 1999 [in Japanese]

Saeki, E., Maeda, Y., Nakamura, H., Midorikawa, M., and Wada, A., *Experimental Study on Practical-Scale Unbonded Braces*, Journal of Structural and Construction Engineering, Architectural Institute of Japan, Structural Engineering Section, 1992 [in Japanese]

Staker, R., and Reaveley, L.D., *Selected Study on Unbonded Braces*, Proceedings, Seminar on Response Modification Technologies for Performance-Based Seismic Design, 2002

Suzuki, N., Kaneko, H., Higasibata, Y., Sasaki, T., and Segawa, T., *Experimental Study on the H-Section Steel Brace Encased in RC or Steel Tube*, Summaries of technical papers of annual meeting, vol. II. Architectural Institute of Japan, C, Structural Engineering Section, 1994 [in Japanese]

Tada, M., Kuwahara, S., Yoneyama, T., and Imai, K., *Horizontally Loading Test of the Steel Frame Braced with Double-Tube Members*, Annual technical papers of steel structures, vol. I., 1993 [in Japanese]

Tremblay, R., Degrange, G., and Blouin, J., *Seismic Rehabilitation of a Four-Story Building with Stiffened Bracing System*, Proceedings, 8th Canadian Conference on Earthquake Engineering, Vancouver, Canada, 1999

Tremblay, R., Bolduc, P., Neville, R., and Devall, R., *Seismic Testing and Performance of Buckling-Restrained Bracing Systems*, Canadian Journal of Civil Engineering, 2006

Uang, C., and Nakashima M., *Steel Buckling-Restrained Braced Frames*, Earthquake Engineering from Engineering Seismology to Performance Based Engineering, CRC Press, 2004

Watanabe, A., Hitomi, Y., Saeki, E., Wada, A., and Fujimoto,M., *Properties of Brace Encased in Buckling-Restraining Concrete and Steel Tube*, Proceedings, 9th World Conference on Earthquake Engineering, vol. IV., 1988

Xie, Q., *State of the Art of Buckling-Restrained Braces in Asia*, Journal of Constructional Steel Research, 2005